Epidermal mammalian target of rapamycin complex 2 controls lipid synthesis and filaggrin processing in epidermal barrier formation

Xiaolei Ding, PhD,[a,b] Sebastian Willenborg, PhD,[a] Wilhelm Bloch, PhD,[c] Sara A. Wickström, MD, PhD,[d,e,f,g] Prerana Wagle, MSc,[g] Susanne Brodesser, PhD,[g] Axel Roers, MD,[h] Alexander Jais, PhD,[i] Jens C. Brüning, MD,[b,g,i] Michael N. Hall, PhD,[j] Markus A. Rüegg, PhD,[j] and Sabine A. Eming, MD[a,b,g] *Cologne and Dresden Germany, Helsinki, Finland, and Basel, Switzerland*

GRAPHICAL ABSTRACT

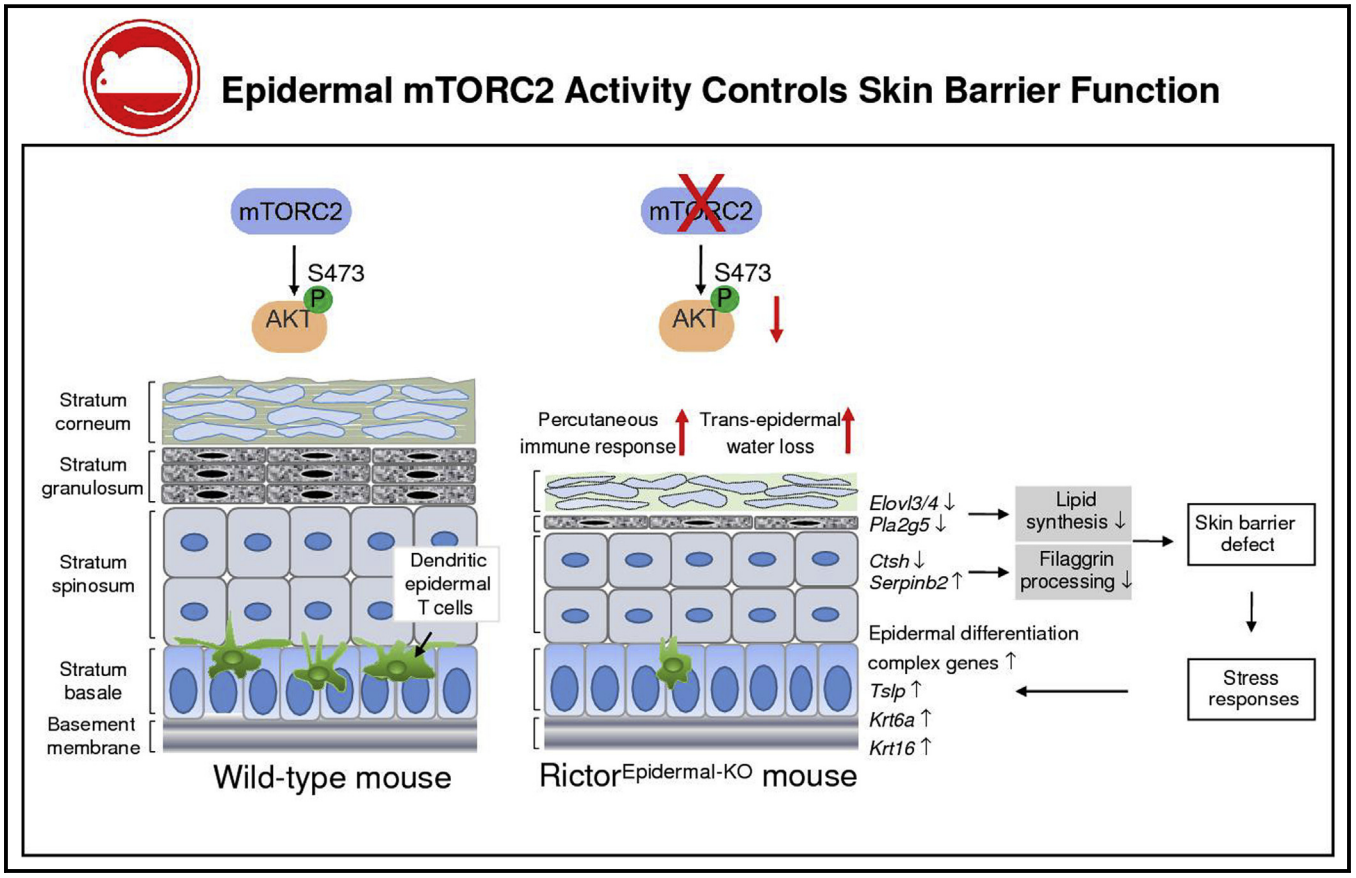

From [a]the Department of Dermatology, [b]the Center for Molecular Medicine Cologne (CMMC), and [g]the Cluster of Excellence Cellular Stress Responses in Aging-associated Diseases (CECAD), University of Cologne; [c]the Department of Molecular and Cellular Sport Medicine, German Sport University Cologne; [d]the Paul Gerson Unna Group "Skin Homeostasis and Ageing," Max Planck Institute for Biology of Ageing, Cologne; [e]the Helsinki Institute of Life Science and [f]the Wihuri Research Institute, Biomedicum Helsinki, University of Helsinki; [h]the Institute for Immunology, Medical Faculty Carl Gustav Carus, TU Dresden; [i]the Max Planck Institute for Metabolism Research, Cologne; and [j]Biozentrum, University of Basel.

The funding source for this article was the Deutsche Forschungsgemeinschaft (Projektnummer 73111208-SFB829 and CECAD to S.A.E., S.A.W., and J.C.B. and FOR2599 to S.A.E. and A.R.) and the Center for Molecular Medicine Cologne (to S.A.E.).

Disclosure of potential conflict of interest: The authors declare that they have no relevant conflicts of interest.

Received for publication January 25, 2019; revised June 21, 2019; accepted for publication July 8, 2019.

Available online August 8, 2019.

Corresponding author: Sabine A. Eming, MD, Department of Dermatology, University of Cologne, Kerpenerstr 62, 50937 Cologne, Germany. E-mail: sabine.eming@uni-koeln.de.

0091-6749/$36.00

https://doi.org/10.1016/j.jaci.2019.07.033

Background: Perturbation of epidermal barrier formation will profoundly compromise overall skin function, leading to a dry and scaly, ichthyosis-like skin phenotype that is the hallmark of a broad range of skin diseases, including ichthyosis, atopic dermatitis, and a multitude of clinical eczema variants. An overarching molecular mechanism that orchestrates the multitude of factors controlling epidermal barrier formation and homeostasis remains to be elucidated.

Objective: Here we highlight a specific role of mammalian target of rapamycin complex 2 (mTORC2) signaling in epidermal barrier formation.

Methods: Epidermal mTORC2 signaling was specifically disrupted by deleting rapamycin-insensitive companion of target of rapamycin *(Rictor)*, encoding an essential subunit of mTORC2 in mouse epidermis (epidermis-specific homozygous Rictor deletion [Ric^{EKO}] mice). Epidermal structure and barrier function were investigated through a combination of gene expression, biochemical, morphological and functional analysis in Ric^{EKO} and control mice.

Results: Ric^{EKO} newborns displayed an ichthyosis-like phenotype characterized by dysregulated epidermal *de novo* lipid synthesis, altered lipid lamellae structure, and aberrant filaggrin (FLG) processing. Despite a compensatory transcriptional epidermal repair response, the protective epidermal function was impaired in Ric^{EKO} mice, as revealed by increased transepidermal water loss, enhanced corneocyte fragility, decreased dendritic epidermal T cells, and an exaggerated percutaneous immune response. Restoration of Akt-Ser473 phosphorylation in mTORC2-deficient keratinocytes through expression of constitutive Akt rescued FLG processing.

Conclusion: Our findings reveal a critical metabolic signaling relay of barrier formation in which epidermal mTORC2 activity controls FLG processing and *de novo* epidermal lipid synthesis during cornification. Our findings provide novel mechanistic insights into epidermal barrier formation and could open up new therapeutic opportunities to restore defective epidermal barrier conditions. (J Allergy Clin Immunol 2020;145:283-300.)

Key words: *Epidermal barrier, mammalian target of rapamycin complex 2, Rictor, ichthyosis, filaggrin, epidermal lipid synthesis*

Abbreviations used

7-AAD: 7-Amino-actinomycin D
ACD: Allergic contact dermatitis
AD: Atopic dermatitis
APC: Allophycocyanin
CE: Cornified envelope
DETC: Dendritic epidermal T cell
DNFB: 1-Fluoro-2,4-dinitrobenzene
FACS: Fluorescence-activated cell sorting
FFA: Free fatty acid
FITC: Fluorescein isothiocyanate
FLG: Filaggrin
GFP: Green fluorescent protein
ICD: Irritant contact dermatitis
Krt: Keratin
LB: Lamellar body
mTOR: Mammalian target of rapamycin
mTORC: Mammalian target of rapamycin complex
myr-AKT: Myristoylated Akt1
PE: Phycoerythrin
qRT-PCR: Quantitative RT-PCR
Ric^{EKO}: Epidermis-specific homozygous Rictor deletion
Rictor: Rapamycin-insensitive companion of target of rapamycin
SC: Stratum corneum
SG: Stratum granulosum
TCR: T-cell receptor
TEM: Transmission electron microscopy
TEWL: Transepidermal water loss

The epidermis is a stratified squamous epithelium that provides a life-sustaining permeability barrier preventing water loss and protecting the body from a plethora of physical and chemical insults, as well as pathogenic microorganisms.[1] Perturbation of epidermal barrier function will profoundly compromise overall skin barrier function, frequently leading to a dry and scaly, ichthyosis-like skin phenotype, which is the hallmark of a broad range of skin diseases, including ichthyosis, atopic dermatitis (AD), and a multitude of clinical eczema variants associated, for example, with diabetes mellitus or aging.[2-4] Quality of life is frequently negatively affected, and patients are also at high risk for associated morbidity and mortality.[5] The molecular mechanisms regulating proper barrier function and maintenance are not yet understood, and this was the aim of this study.

Epidermal barrier function is acquired and maintained by a tightly regulated keratinocyte differentiation process known as cornification. The innermost mitotically active cell layer, the stratum basale, undergoes continuous proliferation and differentiation, providing cells to the above stratum spinosum, stratum granulosum (SG), and the stratum corneum (SC). The outermost SC makes up most of the permeability barrier. The SC consists of flattened, anuclear, and keratin-filled corneocytes embedded in an intercellular lipid-rich matrix composed of ceramides, cholesterol, and free fatty acids (FFAs) in an acidic environment.[2,6] Perturbation of cornification will profoundly compromise skin barrier function.[2,6]

Genetic analyses have established a strong link between genetic defects and skin barrier disorders in both human subjects and mice, providing the basis for the current understanding of molecular networks orchestrating cornification.[7] Of particular importance was the discovery of loss-of-function mutations in the filaggrin *(FLG)* gene, the cause of the most common genodermatosis, namely ichthyosis vulgaris, which is characterized by dry scaly skin.[8,9] Ichthyosis vulgaris has been identified as a predisposing factor for the development of AD, the most common chronic inflammatory skin disease, affecting up to 20% of children and 7% to 10% of adults.[10] However, a significant number of patients with AD have no *FLG* mutations, and recent human genetic studies suggest that a reduction in profilaggrin expression at the protein level can lead to skin barrier defects, suggesting that other mechanisms and candidate molecules might regulate profilaggrin expression and proteolytic processing.[9,11]

Furthermore, the identification of mutations in diverse *Elovl* genes in mice and pediatric patients with AD, encoding very long-chain fatty acid elongases, revealed a central role for *de novo* ceramide synthesis in cornification and proper epidermal

barrier function.[1,10,12-14] In addition, *Pla2g5* activity catalyzes FFA synthesis and has been shown to be critical in epidermal barrier formation.[15] However, the overarching molecular mechanisms that orchestrate the multitude of factors controlling keratinocyte fate and cornification are not known.[16,17]

Recently, we identified the serine/threonine protein kinase mammalian (also known as mechanistic) target of rapamycin (mTOR) as an essential regulator of epidermal differentiation and barrier formation in embryonic development.[18,19] Here we hypothesized that mammalian target of rapamycin complex (mTORC) 2 plays a critical role in postnatal epidermal barrier assembly and maintenance. mTOR is a central regulator of cell growth and metabolism and is evolutionarily highly conserved.[20,21] mTOR assembles in 2 structurally and functionally distinct multiprotein complexes referred to as mTORC1 and mTORC2.[20,21] The rapamycin-insensitive companion of target of rapamycin (Rictor) protein is an essential and specific subunit of mTORC2. Growth factors are able to stimulate mTORC2 kinase activity, and activated mTORC2 phosphorylates several members of the AGC kinase family, including AKT, specifically at Ser473 (AKT-pSer473) to control cell metabolism and cytoskeletal organization.[22,23] In the setting of keratinocyte differentiation, AKT activity is induced, regulating FLG expression and processing.[24,25] Interestingly, a recent study showed that increased expression of Raptor, the regulatory-associated protein of mTORC1, correlates with reduced AKT activity and FLG expression in the skin of patients with AD.[26]

In this study we assessed the role of epidermal mTORC2 in postnatal skin barrier function by inactivating *Rictor* in the mouse epidermis. We show that mTORC2 promotes nonredundant functions for proper cornification through regulation of epidermal lipid metabolism and FLG processing. Our findings could suggest a new therapeutic strategy to regulate epidermal barrier function and to prevent complications in patients with dry skin diseases.

METHODS

Mice

Epidermal-specific *Rictor* knockout mice (C57BL/6) were generated by crossing mice carrying loxP-flanked *Rictor* alleles with a Cre-transgenic strain expressing Cre recombinase under control of the human keratin 14 promoter (see Fig E1, *A*, in this article's Online Repository at www.jacionline.org).[18] Littermates that either lacked Cre or expressed Cre but carried a heterozygous loxP-flanked *Rictor* allele served as control mice. Genotyping was performed, as previously described.[18] Mice were maintained and bred under standard pathogen-free conditions. All procedures were approved by the North Rhine-Westphalian State Agency for Nature, Environment, and Consumer Protection and the University of Cologne.

Histologic analysis

Skin tissues were fixed in 4% paraformaldehyde, embedded in paraffin, and sectioned (10 μm). Hematoxylin and eosin staining was performed according to a standard procedure.[27] Images were analyzed with a light microscope (Leica DM4000B; Leica Microsystems, Wetzlar, Germany).

Separation of epidermis from mouse back skin

Subcutaneous fat tissue was mechanically dissected from excised back skin. The epidermis was separated from the dermis after floating skin biopsies in 0.5 mol/L ammonium thiocyanate in phosphate buffer, pH 6.8 (0.1 mol/L NH_2HPO_4, and 0.1 mol/L KH_2PO_4), for 30 minutes on ice epidermis side up. The epidermis was used for either RNA isolation, biochemical analysis, or immunostaining.

Immunostaining

For immunohistochemical and immunofluorescence staining, cryosections from Optimal Cutting Temperature compound (Tissue Tek; Sakura Finetek, Torrance, Calif)–embedded tissues were fixed (4% paraformaldehyde or in methanol), blocked (10% normal goat serum in PBS), and incubated with primary antibodies (diluted in blocking buffer) overnight at 4°C. Bound primary antibody was detected by means of incubation with peroxidase-conjugated (EnVision System; Dako, Glostrup, Denmark) secondary antibody, followed by incubation with peroxidase substrate (Sigma, St Louis, Mo) or Alexa Fluor 488– or Alexa Fluor 594–conjugated antibodies (Invitrogen, Carlsbad, Calif). Nuclei were counterstained with hematoxylin or 4′,6-diamidino-2-phenylindole (Invitrogen). After washing, slides were mounted in mounting medium. For whole-mount staining, the epidermis was separated from the ears, as described above. Epidermal sheets were fixed with acetone and stained with anti-γδ T-cell receptor (TCR) antibody. Images were taken with a Zeiss Meta 710 Confocal Microscope (Zeiss, Oberkochen, Germany) or KEYENCE Fluorescence Microscope (BZ-9000; KEYENCE, Osaka, Japan). Antibody information can be found in Table E1 in this article's Online Repository at www.jacionline.org.

For quantification of phosphorylated Akt-S473 staining, 3 representative high-power fields per section were quantified with ImageJ software (https://imagej.nih.gov/ij/index.html), as described previously.[27] Findings are expressed as the percentage of phosphorylated Akt-S473–stained areas within the ear epidermis. Numbers of inflammatory cells were determined by counting positively stained cells in 5 representative high-power fields (×400 magnification) per section. Analyses were performed in a blind manner by 2 independent investigators.

Transmission electron microscopy

Skin tissues were isolated and fixed in buffer (2% paraformaldehyde, 2% glutaraldehyde, and 0.1 mol/L cacodylate buffer at pH 7.35) and postfixed with ruthenium tetroxide. Tissue embedding and ultrathin section preparations were performed, as previously described.[28]

Flow cytometry and cell sorting

For analysis of immune cells, single-cell suspensions of skin from control and epidermis-specific homozygous Rictor deletion (Ric^{EKO}) mice were prepared by using a combination of enzymatic digestion (Liberase Blendzyme, Roche Applied Science, Penzberg, Germany) and mechanical disruption (Medimachine System; BD Biosciences, San Jose, Calif), as previously described.[28] For flow cytometric analysis, cells were stained, as described previously.[28] Briefly, cells were passed through a 40-μm cell strainer, washed with PBS, and incubated with the following antibodies: eFluor 450– or allophycocyanin (APC)–eFluor 780–conjugated anti-CD45 (clone 30-F11; eBioscience, San Diego, Calif), APC-Cy7–conjugated anti-CD4 (clone GK1.5; BD PharMingen), phycoerythrin (PE)– or PE-Cy7–conjugated anti-CD3e (clone 145-2C11; eBioscience), PE-conjugated anti–Siglec-F (clone E50-2440; BD PharMingen), fluorescein isothiocyanate (FITC)– or BV421–conjugated anti-γδTCR (clone GL3; BD PharMingen), FITC-conjugated anti-Vγ3 TCR (clone 536; BD PharMingen), FITC-conjugated anti-F4/80 (clone Cl:A3-1; Bio-Rad Laboratories, Hercules, Calif), or APC-Cy7–conjugated Ly-6G (clone E50-2440; BD PharMingen) in fluorescence-activated cell sorting (FACS) buffer. Dead cells were excluded by using 7-amino-actinomycin D (7-AAD; BD Biosciences). Cells were analyzed on a FACSCanto II flow cytometer (BD, Franklin Lakes, NJ), which was equipped with FACSDiva software (BD). For flow cytometric sorting, green fluorescent protein $(GFP)^+$ keratinocytes were sorted by using the FACSAria cell sorting system (BD).

RNA transcriptomics and gene set enrichment analysis

Total RNA was extracted from separated epidermal tissue by using the RNeasy Mini Kit (Qiagen, Hilden, Germany), and RNA quality was determined with an Agilent 2200 TapeStation (Agilent Technologies, Santa Clara, Calif). Preparation of amplification reactions of cDNA was performed

at the Cologne Center for Genomics by using the Ovation RNA-Seq System V2 (NuGen, Redwood City, Calif), and the library was prepared by using the Nextera XT library preparation kit (Illumina, San Diego, Calif). RNA sequencing was carried out on Illumina HiSeq2000 machines by using the 2_100-bp protocol and V3 chemistry. After quality control, adapter sequences were removed with flexbar63. Reads mapping to rRNA-related genes were filtered out by using a custom ribosomal RNA-only reference. After preprocessing, reads were mapped to the *Mus musculus* reference genome (build GRCm38_79), followed by differential gene expression analysis with the DESeq2 R library (version 1.6.3). Hierarchical clustering was performed in R software. Transcripts that regulated greater than 1.5-fold with a *P* value of less than .05 were used in Gene Ontology term analysis (DAVID Bioinformatics Resources 6.8) to identify enriched functional annotations. Gene set enrichment analysis was performed on the whole gene list and compared with the Broad Institute Molecular Signatures Database collection of chemical and genetic perturbations (C2) by using the Web-based tool available from the Broad Institute.[29] Enrichments with a false discovery rate value of less than 0.05 were considered significant. RNA-seq data sets of this study have been submitted to the Gene Expression Omnibus database (http://www.ncbi.nlm.nih.gov/geo) under the accession number GSE133295.

Cornified envelope isolation for microscopy

A defined area of dorsal mouse skin (25 mm^2) was boiled in isolation buffer (20 mmol/L Tris-HCl [pH 7.5], 5 mmol/L EDTA, 10 mmol/L dithiothreitol, and 2% SDS) under vigorous shaking for 40 minutes. After centrifugation, the cornified envelopes (CEs) were washed twice with isolation buffer and analyzed with a hemocytometer.[30]

Lipid analysis

For analysis of SC lipids, the SC was separated from the back skin of newborn mice by floating the skin with the dermis side down on 0.5% trypsin in PBS for 24 hours at 37°C.[31] The SC was washed in PBS, lyophilized, and weighed. Lyophilized SC was homogenized in 0.5 mL of water by using the Precellys 24 Homogenisator (Peqlab, Erlangen, Germany) at 6500 rpm for 30 seconds. After addition of 0.5 mL of water and 2 mL of chloroform/methanol 1:2 (vol/vol), freely extractable SC lipids were extracted for 24 hours at 37°C and purified by using a modification of the Bligh-Dyer procedure, as previously described.[32] For lipid quantification, the equivalent of 1.1 mg of lyophilized SC was loaded on 20 × 10–cm high-performance thin-layer chromatography plates, which were developed twice in chloroform/methanol/glacial acetic acid 190:9:1 (vol/vol/vol). Quantitative analytic thin-layer chromatography determination was performed, as previously described.[33] Nile red staining was performed on cryosections for 2 minutes with 0.2 mg/mL Nile red in 75% glycerol; the fluorescence intensity of Nile red–stained epidermis was determined by means of integrated density with ImageJ software.

Transepidermal water loss measurements

Transepidermal water loss (TEWL) measurements were carried out, as described previously,[18] with a Tewameter (Courage and Khazaka Electronic GmbH, Cologne, Germany), and the measurements were performed according to the manufacturer's instructions.

Irritant and allergic contact dermatitis

The inner and outer surfaces of the right ear were treated with 5 μL of 1% croton oil in acetone/olive oil (4:1) to assess irritant contact dermatitis (ICD). The left ear was treated with acetone/olive oil only and taken as a control. Ear thickness was measured 4, 8, and 24 hours after the treatment by using a digital caliper. Ear swelling was determined by calculating the changes in ear thickness between the challenged ear (right) and the control ear (left).

Mice were sensitized by painting 25 μL of 1% 1-fluoro-2,4-dinitrobenzene (DNFB; Sigma) in acetone/olive oil (4:1) onto the shaved abdominal skin at day 0 to evaluate hapten-induced allergic contact dermatitis (ACD). At day 6, mice were challenged by applying 5 μL of 0.4% DNFB in acetone/olive oil on the inner and outer surfaces of the right ear, respectively. The left ear was treated with acetone/olive oil only and taken as a control. Ear thickness was measured 8, 24, and 48 hours after treatment with a digital caliper. Ear swelling was determined by calculating the changes in ear thickness between the challenged ear (right) and control ear (left).

Cell culture

Keratinocytes were isolated from newborns and cultured in low Ca^{2+} medium, as described previously.[27] Briefly, skin was floated dermal side down on 0.25% trypsin solution (Gibco, Carlsbad, Calif) for 16 hours at 4°C. The epidermis was separated from the dermis and minced with a scalpel. Cell and epidermal tissue were suspended, shaken for 30 minutes at 37°C, and seeded on collagen-coated 6-well plates with mitomycin C (Sigma)–treated 3T3 fibroblast feeder layer cells. For induction of keratinocyte differentiation, medium was supplemented with 0.2 mmol/L $CaCl_2$ (high Ca^{2+} medium).

Plasmids, viral preparation, and keratinocyte infection

MSCV-IRES-GFP retrovirus vector with myristoylated Akt1 (myr-AKT) was used, as described previously.[34] myr-AKT–IRES–GFP and IRES-GFP retroviral supernatants were produced in 293T cells, as previously described.[35] Briefly, 293T cells were transfected with vector constructs and packaging plasmids (pVPack-GP and pVPack-Eco; Stratagene, San Diego, Calif). Forty-eight hours after transfection, viral supernatant was harvested and concentrated by means of precipitation with chondroitin 6-sulfate (Sigma) and Polybrene (Sigma) and centrifuged. Keratinocytes (P2) were exposed to concentrated viruses for 24 hours, and GPF^+ cells were sorted by using flow cytometry.

Quantitative RT-PCR analysis

RNA from the epidermis and skin was extracted by using an RNA isolation kit (Qiagen), according to the manufacturer's instructions. Reverse transcription of isolated RNA was performed with the High Capacity cDNA RT Kit (Applied Biosystems, Foster City, Calif). Amplification reactions were performed with PowerSYBR Green PCR Master Mix (Applied Biosystems) using a 7300 Real Time PCR system (Applied Biosystems). The comparative method of relative quantification ($2^{-\Delta\Delta}$ cycle threshold) was used to calculate the expression level of the target gene normalized to glyceraldehyde-3-phosphate dehydrogenase. Primer sequence information can be found in Table E2 in this article's Online Repository at www.jacionline.org.

Western blot analysis

The epidermis was separated from the dermis and dissociated with a Mixer Mill (Retsch GmbH, Haan, Germany). For analysis of FLG, loricrin, and keratin, the epidermis was lysed in a 4% SDS lysis buffer. Alternatively, cells or tissues were lysed in RIPA buffer containing protease inhibitor (Sigma-Aldrich) and phosphatase inhibitor (Roche, Mannheim, Germany). Protein concentrations were determined by using the Micro BCA Protein Assay Kit (Thermo Scientific, Waltham, Mass), and 20 mg of protein per sample was subjected to SDS-PAGE (Invitrogen). Subsequently, protein was blotted to polyvinylidene difluoride membranes. After blocking (5% nonfat milk in TBS-Tween buffer), membranes were incubated with primary antibodies. Antibody information can be found in Table E1.

For densitometric analysis, enhanced chemiluminescence–exposed film was scanned and quantified with ImageJ software. Briefly, images were converted to grayscale, and the background was removed. Densitometry was achieved by using the Gel Analysis method with ImageJ software. Ratios of FLG monomer and total FLG, profilaggrin, and β-actin were determined with control set to 1, or relative intensity was calculated after normalizing to a loading control (β-actin).

Statistical analysis

Data are presented as means ± SEMs, and statistics were performed with Prism software (version 5.0a; GraphPad Software, La Jolla, Calif). Statistical significance of the difference was determined by using the unpaired 2-tailed Student *t* test or 1-way ANOVA with Bonferroni multiple comparison. A *P* value of less than .05 was considered statistically significant.

RESULTS

Ric^{EKO} mice display a transient ichthyosis-like phenotype

To explore the role of epidermal mTORC2 signaling, we knocked out *Rictor* specifically in the epidermis, as previously described.[18] Briefly, mice carrying a loxP-flanked *Rictor* allele were crossed with a transgenic mouse expressing Cre recombinase under the control of the human keratin 14 promoter,[36,37] leading to epidermis-specific deletion of *Rictor* (Ric^{EKO}) in all basal cells and their progeny (see Fig E1, *A*). Epidermis-specific Cre-mediated recombination of floxed *Rictor* alleles, which was verified by using PCR analysis of genomic DNA extracted from different organs, including the epidermis, resulted in effective epidermal loss of Rictor protein expression, as confirmed by using Western blot analysis and immunohistochemical staining (Fig 1, *A*, and see Fig E1, *B* and *C*).

Immediately after birth, Ric^{EKO} mice were clearly distinguishable from their wild-type littermates, exhibiting shiny, translucent, and fragile skin. Occasionally, Ric^{EKO} newborns showed small erosions at the trunk, which might have occurred because of mechanical stress of the skin during birth. This skin fragility might have led to the observed death of approximately 20% of the mutant mice before or after weaning (see Fig E1, *D*).

By day postnatal 7 (P7), a prominent phenotype of dry and scaly, ichthyosis-like skin was apparent, often beginning with scaling of the ventral side already around P3 (Fig 1, *B*). Histologic analysis revealed a stratified epidermis but significantly reduced epidermal thickness in Ric^{EKO} pups at P4 (Fig 1, *C*). Epidermal atrophy was primarily caused by reduced granular cell layers and thinner SC. In addition, the SC in Ric^{EKO} mice displayed structural defects, including poor organization of upper SC layers and densely packing of lower layers compared with the well-defined basket weave–like structure in control mice (Fig 1, *C*). Although less pronounced, the epidermal atrophy remained detectable in adults (P70, see Fig E1, *E*).

Morphologic alterations in the epidermis in Ric^{EKO} newborns were paralleled by a transient impairment of epidermal barrier function, as revealed by a significant increase in TEWL in P4 mutants (Fig 1, *D*, and see Fig E1, *F*). As assessed by means of immunofluorescent staining for multiple tight/adherent junction proteins and components of desmosomal plaques, intercellular junctions appeared to be similar in control and Ric^{EKO} epidermis (see Fig E1, *G*). Ric^{EKO} mice were born at the expected Mendelian ratio and exhibited normal body weight at birth, yet their weight by P5 decreased by 20% compared with littermate control mice; the smaller body size persisted throughout adulthood (Fig 1, *E*, and see Fig E1, *H*).

Ric^{EKO} mice display increased corneocyte fragility

CEs were prepared from the back skin of control and Ric^{EKO} mice at P4 to test whether epidermal atrophy and mechanical fragility in young Ric^{EKO} mice was associated with decreased physical resistance of the SC. Notably, 80% of CEs isolated from control mice remained in a uniformly rigid, large, and intact polygonal shape, whereas more than 60% of Ric^{EKO} CEs were ruptured, irregular, and fragmented, which is indicative of significant fragility and structural defects (Fig 1, *F*).

Ultrastructural analysis of P5 epidermis by using transmission electron microscopy (TEM) showed that the inner portion of Ric^{EKO} epidermis, including the basement membrane, stratum basale, and stratum spinosum, as well as desmosomal plaques, were not grossly affected (see Fig E1, *I*). However, detailed inspection revealed that keratin intermediate filaments in mutant mice were not condensed and were more loosely packed compared with those in control mice (Fig 1, *G*), which might contribute to the reduced resistance to mechanical stress in Ric^{EKO} CEs. Together, our findings demonstrate major structural defects in formation of the SG and SC in the absence of epidermal mTORC2 activity.

Epidermal mTORC2 deficiency induces a compensatory transcriptional epidermal repair program in Ric^{EKO} mice

To identify specific genes and pathways mediating mTORC2 signaling and orchestrating the SG to SC transition, we performed an RNA-sequencing (RNA-seq) transcriptomic analysis of epidermis from mutant and control embryos at E19.5, when epidermal maturation nears completion and epidermal gene expression is not influenced by exposure to environmental insults that could mask primary mechanistic effects.

A 1-way ANOVA was performed to calculate the most variable and differentially expressed genes between both sets of epidermal tissue (fold change > 2, $P < .05$). Analysis revealed 231 and 249 genes downregulated and upregulated, respectively, in Ric^{EKO} versus control epidermis (Fig 2, *A*). To identify biological processes underlying the observed gene expression alterations, we performed Gene Ontology enrichment analysis and pathway enrichment analysis of the differentially expressed genes at the 1.5-fold cutoffs by using DAVID 6.8 software. The upregulated gene set was particularly enriched in genes involved in peptide cross-linking (eg, late cornified envelope 3a/b *[Lce3a/b]*, small proline-rich protein 1a *[Sprr1a]*, and *Sprr2h*), keratinization (eg, keratin 6a *[Krt6a]* and *Krt16*), keratinocyte differentiation (eg, stratifin [*Sfn*], *Sprr1a*, and *Lce3a*), and wound repair (eg, *Krt6a*, *Krt16*, and *S100a8*) among others. The downregulated gene set was highly enriched for immune regulators (eg, 2′-5′ oligoadenylate synthetase 1F [*Oas1f*]) and lipid metabolism (eg, *Elovl3/4*, *Pnpla5*, and *Pla2g5*; false discovery rate < 0.05; Fig 2, *A* and *B*).

One of the most striking features of the RNA-seq data was upregulation of genes for late keratinocyte differentiation and SC components, including small proline-rich proteins, late cornified envelope proteins, and S100 proteins (Fig 2, *A*). Several of these gene families comprise the epidermal differentiation complex, encoding a dense cluster of genes with protein products that have been identified as major molecular markers and important functional regulators for terminal differentiation in the stratified epidermis (Fig 2, *C*).[38] A panel of differentially regulated genes was confirmed by using quantitative RT-PCR (qRT-PCR) analysis, validating the RNA-seq data (Fig 2, *D*). Furthermore, gene set enrichment analysis revealed upregulation of stress-response signatures in Ric^{EKO} epidermis compared with

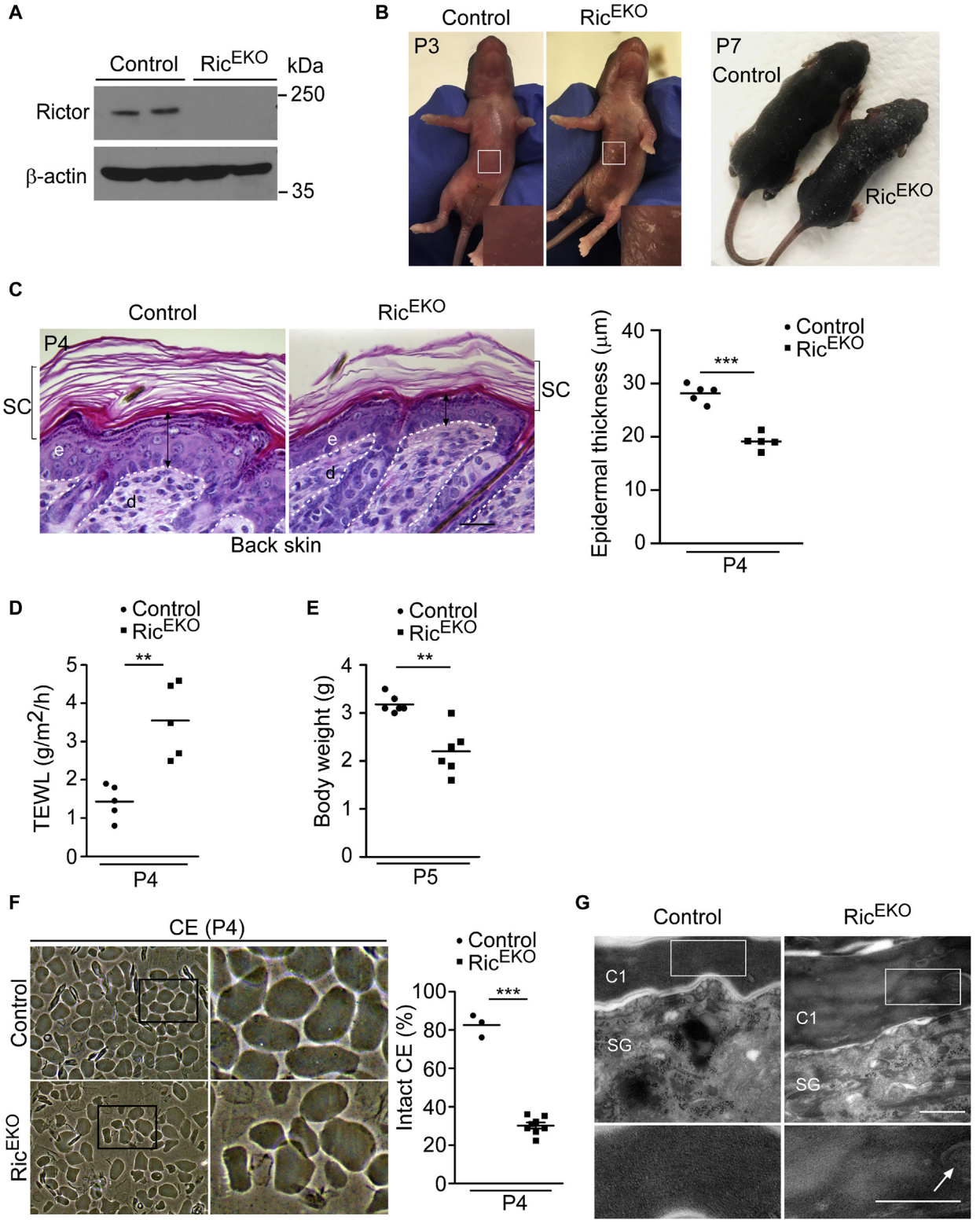

FIG 1. Ric^{EKO} mice display a transient ichthyosis-like phenotype. **A,** Western blot analysis in epidermal isolates at P5. **B,** Macroscopic appearance of littermates. *Boxed areas* are shown at greater magnification. **C,** Hematoxylin and eosin–stained back skin sections at P4 and quantification of epidermal thickness. *d,* Dermis; *e,* epidermis. The *white dashed line* indicates the basal membrane. *Scale bar* = 25 μm. **D,** Quantification of TEWL at P4. Each *dot* or *square* represents 1 mouse. **E,** Body weight at P5. **F,** *Left,* micrographs of isolated CEs from back skin at P4. *Right,* Quantification of the intact CE. Each *dot* or *square* represents isolates from 1 mouse. **G,** TEM image shows poorly condensed SC in Ric^{EKO} mice. Note the presence of cell organelles in C1 of Ric^{EKO} mice (indicated by an *arrow*). *C1,* Cornified layer 1. *Scale bar* = 0.5 μm. Data are expressed as means. The unpaired *t* test was used to calculate *P* values. $^{**}P < .01$ and $^{***}P < .001$.

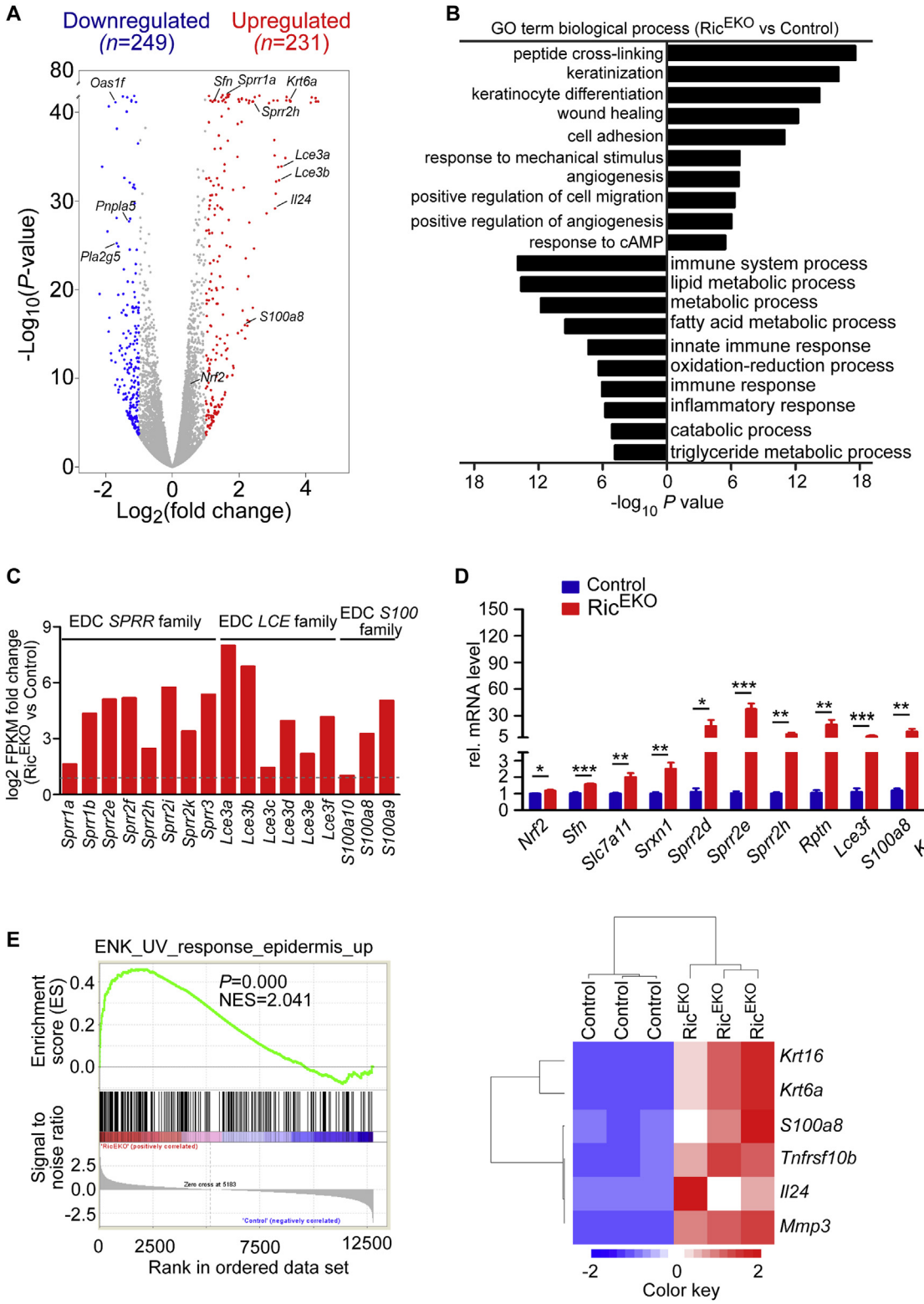

FIG 2. Epidermal mTORC2 deficiency induces a compensatory transcriptional epidermal repair program in Ric^{EKO} mice. **A,** Volcano plot of differentially regulated transcripts between control and Ric^{EKO} epidermis at E19.5 (n = 3 per genotype). *Colored data points* meet thresholds of a $\log_2$ fold change of greater than 1 or less than −1 and an adjusted *P* value of less than .05. **B,** Gene Ontology of differentially regulated transcripts from Ric^{EKO} versus control mice. Comparison was done with DAVID 6.8 online software. Only genes that have a fold change of greater than 1.5 and a *P* value of less than .05 were used. **C,** $\log_2$ fold changes of epidermal differentiation complex *(EDC)* gene expression in the epidermis of Ric^{EKO} skin. EDC genes with an alteration of fold change of greater than 2 and a *P* value of less than .05 are shown. **D,** qRT-PCR analysis validation of differentially expressed genes from RNA-seq data in P0 epidermis (n = 5 per genotype). **E,** *Left,* epidermal UV response gene set enrichment plot in Ric^{EKO} samples. *Right,* Heat map shows the stress-response genes, with positive enrichment in Ric^{EKO} samples. All data are presented as means ± SEMs. The unpaired *t* test was used to calculate *P* values: **P* < .05, ***P* < .01, and ****P* < .001.

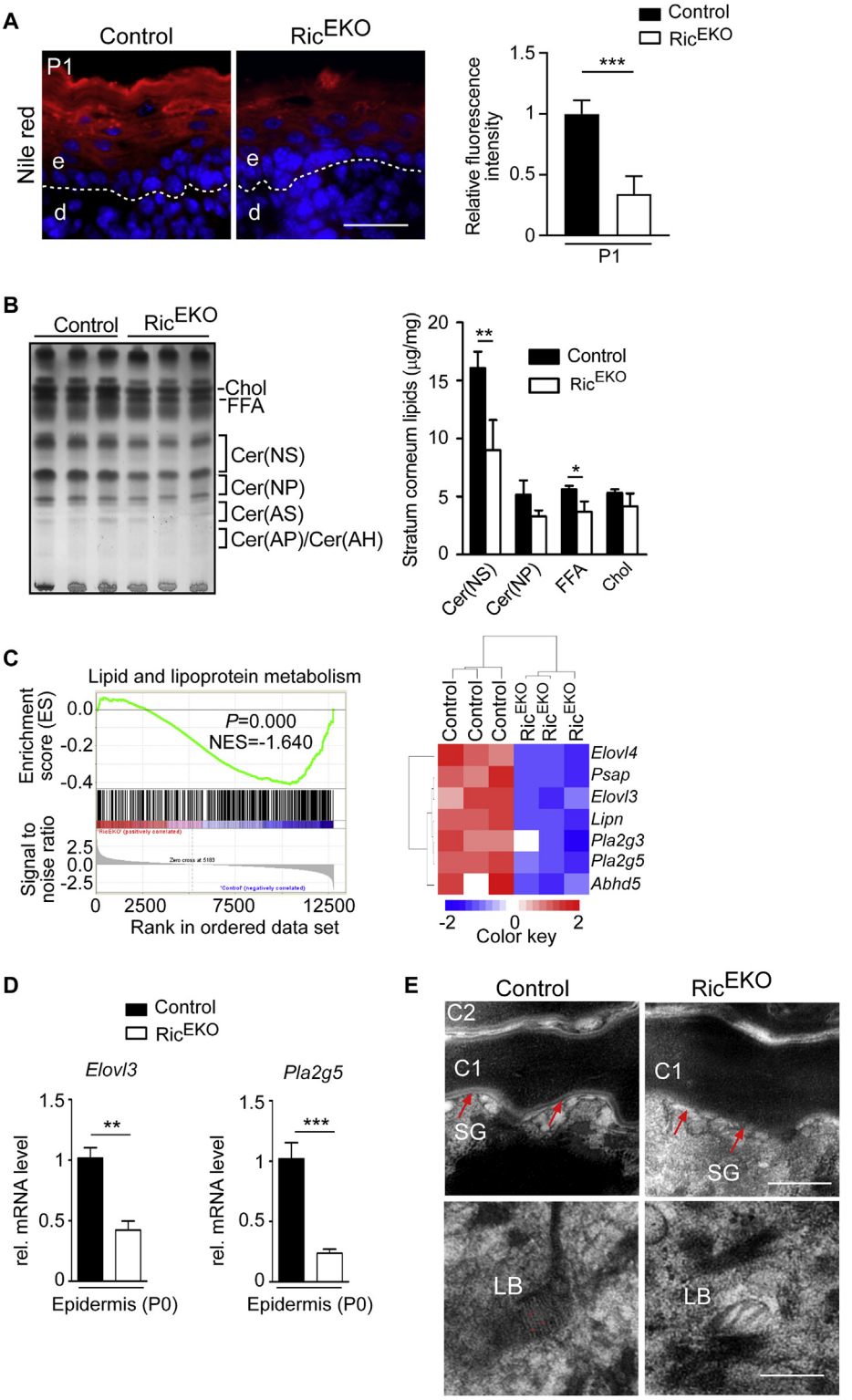

FIG 3. mTORC2 controls epidermal lipid metabolism. **A,** Fluorescent dye Nile red staining and quantification of back skin sections at P1 (n = 4) counterstained with 4′,6-diamidino-2-phenylindole. *d*, Dermis; *e*, epidermis. The *white dashed line* indicates basal membrane. *Scale bar* = 25 μm. **B,** Analysis of SC lipids by using high-performance thin-layer chromatography (n = 3 per genotype). *Cer*, Ceramide; *Chol*, cholesterol. **C,** *Left*, Gene set enrichment analysis of differentially regulated genes between control and Ric^{EKO} epidermis identifies enrichment of lipid and lipoprotein metabolism genes. *Right*, Hierarchically clustered heat map illustration shows differential expression of lipid metabolism–related genes from RNA-seq data. **D,** qRT-PCR analysis of *Elovl3* and *Pla2g5* in the epidermis at P0 (n = 5 per genotype). **E,** Ultrastructural analysis of the interface between SG and SC at P5. Ric^{EKO} epidermis shows a disorganized interface *(red arrows)* between SG and SC and displayed LB abnormalities, including disoriented lamellae and reduced lamellae numbers. In contrast, the LBs of control mice showed regular lamellae orientation with lamellae of equal distance *(red bars)*. *C1*, Cornified layer 1; *C2*, cornified layer 2. *Scale bar* = 200 nm. All data are presented as means ± SEMs. The unpaired *t* test was used to calculate *P* values: **P* < .05, ***P* < .01, and ****P* < .001.

control epidermis, including epidermal barrier stress response regulators (eg, *Krt6a* and *Krt16*)[39] and UVB-induced genes in human epidermis (eg, *S100a8*, *Tnfrsf10b*, *Il24*, and *Mmp3*; Fig 2, *D* and *E*).[40] Collectively, these findings reveal profound alterations in mTORC2-deficient epidermis in gene regulatory networks controlling terminal differentiation and barrier formation and implicate a critical role for mTORC2 activity in formation of a protective epidermal barrier.

mTORC2 controls epidermal lipid metabolism

Keratinocytes of the granular layer contribute to epidermal lipid synthesis, which is essential for effective skin barrier function.[6,41] During cornification, lipids are packed in intracellular lamellar bodies (LBs), which then transport and release lipids into the intercellular space of corneocytes to form a lipid bilayer. The lipid bilayer mainly consists of ceramides, cholesterol, and FFAs.[6] To examine whether the structural and functional SC defects in Ric^{EKO} mice resulted from altered lipid composition, we further analyzed the SC lipid composition. Nile red, a fluorescent lipophilic dye, revealed that the lipid content was markedly diminished in Ric^{EKO} SC (Fig 3, *A*).

Levels of ceramides, cholesterol, and FFAs in the SC were determined by using high-performance thin-layer chromatography to quantify SC lipid composition. The analysis revealed a decrease in all 3 main SC lipid classes in Ric^{EKO} epidermis. In particular, levels of non-hydroxy fatty acid/sphingosine base ceramide (Cer [NS]) in Ric^{EKO} epidermis were decreased by more than 40% compared with control levels (Fig 3, *B*).

Notably, consistent with the reduced SC lipid composition, gene set enrichment analysis of RNA-seq data revealed a panel of lipid metabolism–associated genes, which were significantly downregulated in Ric^{EKO} epidermis. These genes include *Elovl3/4*, *Psap*, *Lipn*, *Pla2g3/5*, and *Abhd5* (Fig 3, *C* and *D*). Of note is that most of these genes have been shown to play a critical role in lipid metabolism and epidermal barrier formation in mice and patients with compromised skin barrier function.[42]

At the interface between the SG and SC, lipid lamellae are released into the intercellular space. We further examined the organization of LBs. In line with the altered epidermal lipid composition, ultrastructural analysis by TEM revealed impaired lipid lamellar structure in the LBs of Ric^{EKO} epidermis. In addition, in Ric^{EKO} epidermis the lipid layer between the SC and SG was disrupted (Fig 3, *E*). Taken together, these findings reveal multiple quantitative defects in SG lipid synthesis that lead to altered lipid composition and LB structure in mTORC2-deficient epidermis, potentially contributing to the compromised epidermal barrier function in Ric^{EKO} mice.

Reduced proteolytic activity is paralleled by impaired FLG processing in mTORC2-deficient epidermis

Intriguingly, further pathway enrichment analysis using the Kyoto Encyclopedia of Genes and Genomes database uncovered highly deregulated lysosomal transcripts in Ric^{EKO} epidermis (Fig 4, *A*). Genetic skin diseases and conditions with disturbed barrier function are often characterized by a disturbed balance of epidermal protease and antiprotease activities.[43] Thus we hypothesized that attenuated proteolytic activity in Ric^{EKO} epidermis might contribute to the disturbed barrier formation and function. Transcripts of several genes encoding members of diverse protease families, such as lysosomal cysteine, aspartic acid, and serine proteinases, were downregulated, including cathepsin H *(Ctsh)* and cathepsin D (*Ctsd*; Fig 4, *B* and *C*). Of interest is that cathepsin H *(CTSH)* and *CTSD* mutations have recently been shown to cause impaired FLG processing and disturbed SC formation.[26,44] Conversely, Serpins, which encode potent protease inhibitors, were upregulated, including *Serpinb2*, which encodes an ovalbumin-like serine protease inhibitor and has been linked to the pathogenesis of certain cornification disorders (Fig 4, *B* and *C*).[45] Moreover, expression of the gene encoding secretory leukocyte peptidase inhibitor *(Slpi)* was markedly increased in Ric^{EKO} epidermis (Fig 4, *D*). *Slpi* encodes an inhibitor of kallikrein 7, a protease required for corneodesmosome cleavage. Interestingly, TEM revealed that corneodesmosomes were retained in Ric^{EKO} epidermis, with an increase in both number and size (Fig 4, *E*), thereby further corroborating attenuated corneodesmosome degradation in the Ric^{EKO} SC, potentially because of reduced Slpi.

Furthermore, proteolytic processing of the CE reinforcement protein profilaggrin is an essential process during proper keratinocyte terminal differentiation.[9] Having found that *Ctsh* and *Ctsd*, encoding 2 proteases critically involved in profilaggrin processing, are downregulated in Ric^{EKO} epidermis, we analyzed profilaggrin protein expression and processing in extracts prepared from control and Ric^{EKO} epidermis using Western blot analysis. Notably, although *FLG* mRNA and profilaggrin protein expression levels were comparable between control and Ric^{EKO} epidermis at P5, the level of FLG monomer was markedly reduced in mutant epidermis, suggesting that decreased epidermal protease activity might affect FLG processing in Ric^{EKO} epidermis (Fig 4, *F* and *G*).

A keratinocyte-autonomous mTORC2-Akt axis controls FLG processing

To tackle the molecular mechanism underlying decreased FLG processing in Ric^{EKO} epidermis, we isolated primary keratinocytes from control and Ric^{EKO} newborn mice and analyzed downstream targets of mTOR pathways during terminal differentiation triggered by Ca^{2+} treatment.[46,47] Ca^{2+} triggered activation of both mTORC1 (pS6-Ser240/244) and mTORC2 (phosphorylated Akt-Ser473) in wild-type keratinocytes (Fig 5, *A*). As expected, the absence of mTORC2 in Ric^{EKO} keratinocytes abolished phosphorylation of Akt-Ser473 in response to Ca^{2+} exposure (Fig 5, *A*). Earlier studies demonstrated that Akt is a critical regulator of profilaggrin processing during keratinocyte differentiation.[24,25] Notably, Western blot analysis revealed a pronounced reduction of processed trimer and monomer FLG in Ric^{EKO} keratinocytes. Signals for other markers of keratinocyte differentiation, including loricrin and keratin 10, appeared unchanged in the knockout mice (Fig 5, *B*).

To better define the role of mTORC2-mediated FLG processing, we retrovirally reconstituted Ric^{EKO} keratinocytes with constitutively active myr-AKT[34] and examined FLG processing. Empty pMSCV-IRES-GFP vector transfection served as a control. Infection efficiencies were determined by means of analysis of IRES-driven GFP expression. GFP^+ cells were sorted by using flow cytometry (FACS), expanded *in vitro*, and subjected to high Ca^{2+}-induced differentiation. Western blot analysis

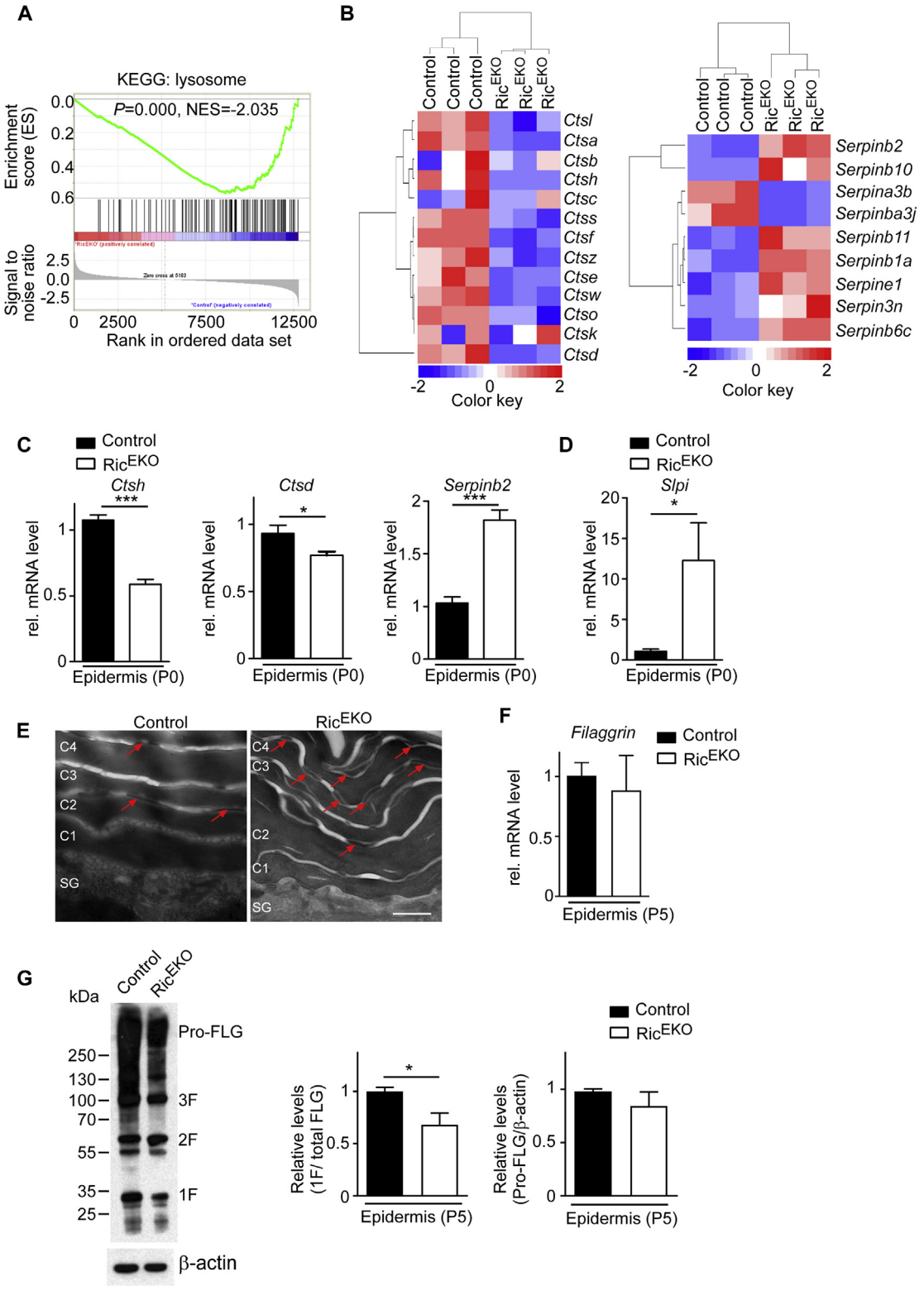

FIG 4. Reduced proteolytic activity and impaired FLG processing in Ric^{EKO} epidermis. **A,** Gene set enrichment analysis of RNA-seq data identifies enrichment of the (Kyoto Encyclopedia of Genes and Genomes) lysosome gene set. **B,** Hierarchically clustered heat map showing altered expression of protease and protease inhibitor genes. **C,** qRT-PCR analysis of indicated genes at P0 (n = 5). **D,** qRT-PCR analysis shows downregulated *Slpi* expression in Ric^{EKO} epidermis (n = 5). **E,** TEM analysis shows delayed corneodesmosome degradation in Ric^{EKO} epidermis at P5. Corneocyte layers *(C)* were numbered, and *arrows* point to corneodesmosomes. *Scale bar* = 200 nm. **F,** qRT-PCR analysis of epidermal *FLG* mRNA expression at P5 (n = 5). **G,** *Left,* Western blot analysis at P5. Profilaggrin *(Pro-FLG),* trimer *(3F),* dimer *(2F),* and monomer *(1F)* FLG are indicated. *Right,* Quantified ratio of FLG monomer *(1F)* and total FLG, profilaggrin, and β-actin with control set to 1 (n = 4). All data are presented as means ± SEMs. The unpaired *t* test was used to calculate *P* values: $*P < .05$, $**P < .01$, and $***P < .001$.

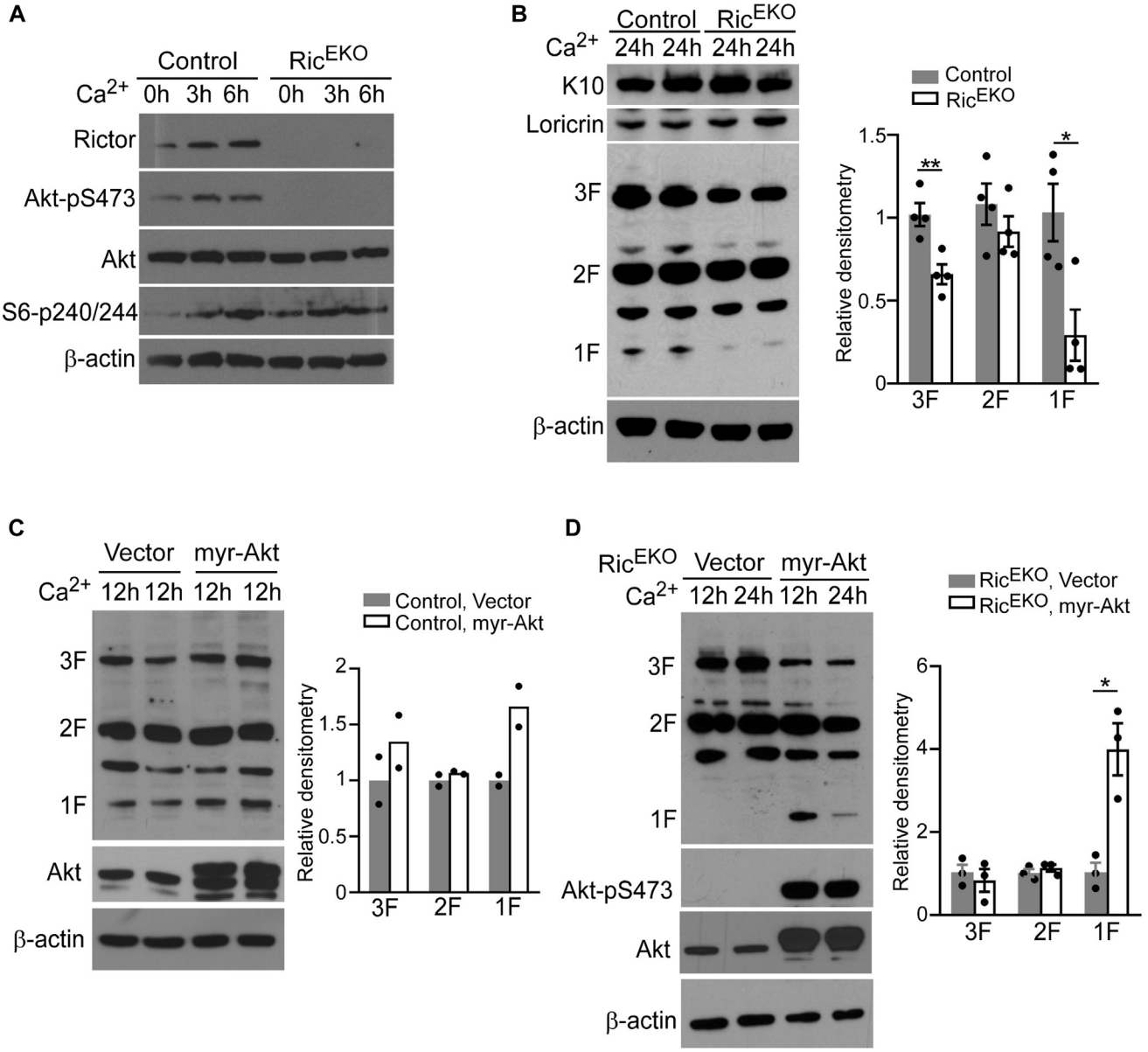

FIG 5. A keratinocyte-autonomous mTORC2-Akt axis controls FLG processing. **A,** Western blot analysis in cultured control and Ric^{EKO} keratinocytes stimulated by a high concentration of Ca^{2+} (0.2 mmol/L). **B,** *Left,* Representative Western blot analysis in keratinocytes. *Right,* Graph of relative densitometry of FLG trimer *(3F),* dimer *(2F),* and monomer *(1F).* **C,** Western blot analysis of FLG and Akt protein expression in empty vector *(Control)*– and myr-Akt retrovirus–infected control keratinocytes. **D,** *Left,* Western blot analysis in empty vector *(Control)*– and myr-Akt retrovirus–infected Ric^{EKO} keratinocytes. *Right,* Graph of relative densitometry of FLG trimer *(3F),* dimer *(2F),* and monomer *(1F).* All data are presented as means ± SEMs. The unpaired *t* test was used to calculate *P* values: **P* < .05 and ***P* < .01.

confirmed abundant myr-AKT protein expression and increased Akt-Ser473 phosphorylation signal in myr-AKT–transduced keratinocytes (Fig 5, *C* and *D*). In line with previous studies,[24,25] enforced myr-Akt expression increased FLG monomer expression in control keratinocytes on calcium-triggered differentiation (Fig 5, *C*). Importantly, restoration of Akt signaling in Ric^{EKO} keratinocytes resulted in a significant increase in the amount of FLG monomer (Fig 5, *D*), indicating that restored Akt-Ser473 phosphorylation enhanced FLG processing in Ric^{EKO} cells. Taken together, our findings implicate mTORC2-mediated activation of Akt-Ser473 as a critical factor in effective FLG processing in keratinocyte terminal differentiation.

Epidermal mTORC2 determines immune cell composition in the skin

Epidermal barrier defects are often associated with altered immune responses and inflammatory skin diseases.[48] To assess the consequences of epidermal mTORC2 deficiency and the

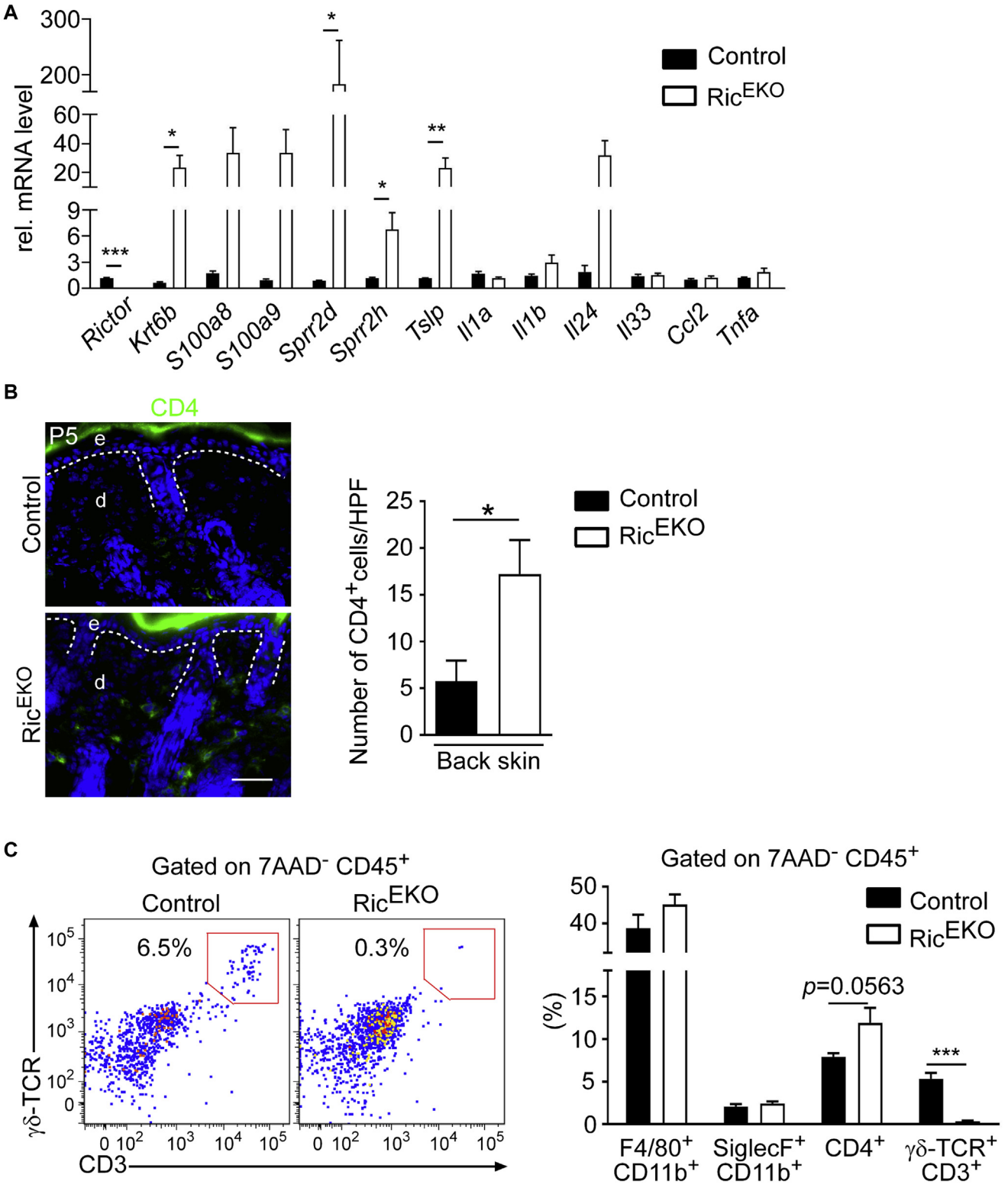

FIG 6. Epidermal mTORC2 determines immune cell composition in the skin. **A,** qRT-PCR profile in epidermis at P5 (n = 8 per genotype). **B,** *Left,* CD4 immunostaining on back skin sections at P5. *Right,* Quantification of $CD4^+$ cells at the high-power field *(HPF). d,* Dermis; *e,* epidermis. The *white dashed line* indicates basal membrane. *Scale bar* = 25 μm. **C,** *Left,* Flow cytometric profile of $\gamma\delta TCR^+CD3^+$ cells at P5. *Right,* Percentage of different cell populations are shown at P5 (n = 6 per genotype). Cells were gated on 7-AAD−$CD45^+$ skin cells. All data are presented as means ± SEMs. The unpaired *t* test was used to calculate *P* values: **P* < .05, ***P* < .01, and ****P* < .001.

resulting barrier defect on immune status, we examined inflammation mediator expression in prenatal E19.5 epidermis (RNA-seq analysis) and in P5 Ric^{EKO} epidermis using qRT-PCR. Notably, although the RNA-seq analysis in prenatal E19.5 epidermis revealed downregulation of inflammation mediators when compared with control values (Fig 2, *B*, and see Table E3 in this article's Online Repository at www.jacionline.org), postnatal (P5) expression of thymic stromal lymphopoietin *(Tslp)* and *Il24* were markedly increased in Ric^{EKO} epidermis compared with littermate control epidermis (Fig 6, *A*). In contrast, transcripts for other potent inflammatory factors, including *Il1α*, *Il1β*, *Il33*, *Ccl2*, and *Tnfa*, were not obviously altered in P5 Ric^{EKO} epidermis (Fig 6, *A*).

To investigate further the effect of epidermal mTORC2 activity on cutaneous immune cell composition, we also performed immunohistochemical and fluorescent analyses in back skin of control and Ric^{EKO} mice at P5. Although no major difference was detected in numbers of toluidine blue–stained mast cells and dermal $F4/80^+$ macrophages, the number of dermal $CD4^+$ T cells was increased in Ric^{EKO} mice (Fig 6, *B*, and see Fig E2, *A*, in this article's Online Repository at www.jacionline.org). The tendency toward an increase in $CD4^+$ cell counts in Ric^{EKO} skin was corroborated by using FACS analysis. Unexpectedly, these analyses further revealed that the percentage of $CD3^+\gamma\delta TCR^+$ cells (gate, $7\text{-}AAD^-CD45^+$) was markedly reduced from 5.314% ± 0.708% to 0.350% ± 0.085% in Ric^{EKO} skin (Fig 6, *C*, and see Fig E2, *B*).

Dendritic epidermal T cells (DETCs) constitute a subset of T cells that express high levels of the γδTCR and specifically localize to the epidermis.[49,50] Consistent with the FACS analysis, immunofluorescent staining for the pan–T-cell marker CD3 revealed a pronounced reduction of epidermal T cells in Ric^{EKO} mice compared with control mice (Fig 7, *A*). Furthermore, epidermal CD3 and γδTCR costaining revealed significantly reduced numbers of DETCs in Ric^{EKO} epidermis (Fig 7, *A*). Intriguingly, RNA-seq analysis of E19.5 Ric^{EKO} epidermis revealed a significant downregulation of several members of the *Skint* family genes when compared with control mice (Fig 7, *B*). γδTCR ligand *Skint* genes are expressed by epidermal keratinocytes and play a critical role in maintaining the DETC pool in the epidermis and in regulating γδTCR cell homeostasis.[51] Downregulated expression of *Skint1* and *Skint4* was confirmed by using qRT-PCR analysis in control und mutant epidermis at P0 (Fig 7, *C*).

To answer the question of whether epidermal mTORC2 activity is important to maintain the homeostasis of DETCs throughout adulthood, we analyzed whole mounts from ear skin in adult mice at P70. Immunofluorescent and FACS analysis revealed that the number of $CD45^+CD3e^+\gamma\delta TCR^{high}V\gamma3^+$ DETCs was also markedly reduced in adult Ric^{EKO} epidermal sheets, whereas the proportion of $CD45^+CD3e^+\gamma\delta TCR^{low}V\gamma3^-$ dermal γδ T cells was similar in Ric^{EKO} and control mice (Fig 7, *D* and E, and see Fig E2, *C*). Interestingly, the majority of DETCs in Ric^{EKO} ears displayed an activated phenotype characterized by a rounded morphology and reduced dendritic spines compared with DETCs in control mice (Fig 7, *D*). Reduced DETC numbers were paralleled by significantly reduced *Skint1* and *Skint4* transcripts (Fig 7, *F*). Collectively, these findings reveal a critical role of epidermal mTORC2 activity in determining the composition of T-cell subpopulations in naive skin.

DNFB-mediated percutaneous immune response is enhanced in Ric^{EKO} mice

Barrier disruption and continuous percutaneous exposure to allergens presumably initiate and drive a variety of inflammatory skin diseases, including AD.[52] In fact, long-term observation under specific pathogen-free conditions revealed mildly dry eyes and perioral dermatitis in Ric^{EKO} mice to a varying extent among individual mutants (see Fig E3, *A*, in this article's Online Repository at www.jacionline.org). Numbers of mast cells, $CD4^+$ T cells, and $F4/80^+$ myeloid cells and transcripts of proinflammatory mediators, including *Il6*, *Tnfα*, *Il1β*, and *Tslp*, showed a tendency toward increased expression, yet the difference did not reach statistical significance in unchallenged back skin of control and mutant mice at 10 weeks (see Fig E3, *B* and *C*). In addition, although serum levels of circulating total IgE were increased in Ric^{EKO} mice at 10 weeks, the difference did not reach statistical significance (see Fig E3, *D*).

To quantify the functional effect of epidermal mTORC2 activity in percutaneous immune responses to exogenous substances, 10-week-old control and Ric^{EKO} mice were subjected to established models of ICD or ACD. Although no difference in ICD was observed between control and mutant mice (see Fig E3, *E*), ACD in response to the hapten DNFB was significantly pronounced in mutant versus control mice (Fig 8, *A*). In control mice the positive DNFB response was paralleled by a significant increase in epidermal phosphorylation of Akt-S473, an alteration of the cellular immune cell infiltrate with a significant increase in numbers of $F4/80^+$ myeloid cells, and a significant decrease in DETC counts (Fig 8, *C*, and see Fig E4 in this article's Online Repository at www.jacionline.org). In contrast, the attenuated DNFB response in Ric^{EKO} epidermis was associated with a significant reduction of epidermal Akt-S473 phosphorylation and an alteration of the cellular immune cell infiltrate, with a significant increase in numbers of granulocytes, $F4/80^+$ myeloid cells, and $CD4^+$ T cells and a virtual absence of DETCs; differences in $F4/80^+$ myeloid cell, $CD4^+$ T-cell, and DETC cell infiltrates were significantly different in Ric^{EKO} versus control mice (Fig 8, *C*, and see Fig E4). In addition, transcripts of stress-response genes, including *Krt6b*, *S100a8*, and *Sprr2d*, and proinflammatory mediators, such as *Il6*, *Tnfα*, and *Il24*, were significantly increased in DNFB-challenged ear skin in Ric^{EKO} versus control mice (see Fig E5 in this article's Online Repository at www.jacionline.org).

Taken together, these findings strongly suggest that the impaired epidermal barrier in Ric^{EKO} mice allows increased hapten penetration, which in turn leads to exaggerated stress and percutaneous immune responses.

DISCUSSION

In the present study we describe epidermal mTORC2 as a central hub orchestrating the complex multicellular crosstalk and signaling required for postnatal epidermal barrier integrity and function. Specifically, we uncover a key role for epidermal mTORC2 activity in assembly of a protective SC (Fig 8, *D*).

A prominent phenotype of Ric^{EKO} mice is the dry, scaly, and ichthyosis-like appearance of skin. A similar phenotype is present in various mouse mutants and human skin diseases with epidermal barrier defects, including ichthyosis, AD and multiple clinical eczema variants.[16,53] Yet an overarching mechanism that

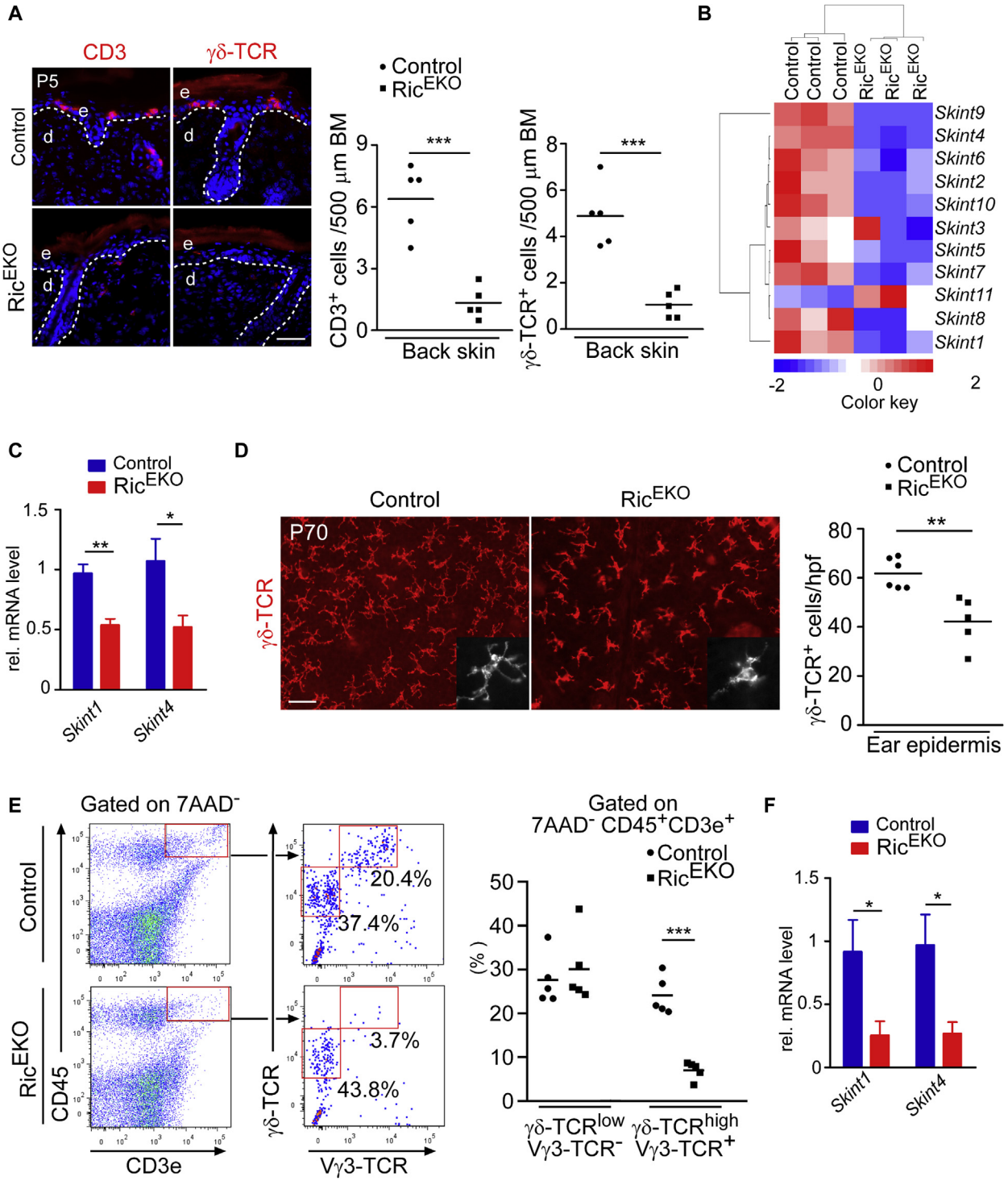

FIG 7. DETC numbers are reduced in Ric^{EKO} epidermis. **A,** *Left*, CD3 and γδTCR immunostaining on back skin at P5. *Right*, quantification of epidermal CD3$^+$ and γδTCR$^+$ cells per 500 μm of basement membrane. The *white dashed line* indicates basal membrane. *Scale bar* = 25 μm. **B,** Hierarchically clustered heat map showing altered expression of *Skint* family genes in Ric^{EKO} epidermis from RNA-seq data. **C,** qRT-PCR analysis validates reduced *Skint1* and *Skint4* expression in Ric^{EKO} epidermis at P0 (n = 5 per genotype). **D,** *Left*, DETCs in epidermis of ear sheet at P70. Separated epidermis was stained against γδTCR. *Right*, Quantification of γδTCR$^+$ cells in epidermal sheets. *Scale bar* = 25 μm. *hpf*, High-power field. **E,** *Left*, Flow cytometry profile of single-cell suspensions of ear skin at P70. 7-AAD$^-$CD45$^+$CD3e$^+$ cells were gated and analyzed for expression of γδTCR and Vγ3-TCR. *Right*, Quantification of γδTCR^{low}Vγ3-TCR$^-$ dermal γδ T cells and γδTCR^{high}Vγ3-TCR$^+$ DETCs. **F,** qRT-PCR analysis of *Skint1* and *Skint4* expression in adult epidermis at P70 (n = 5 per genotype). Each *dot* or *square* represents 1 mouse. Data are presented as means or as means ± SEMs. The unpaired *t* test was used to calculate *P* values: **P* < .05, ***P* < .01, and ****P* < .001.

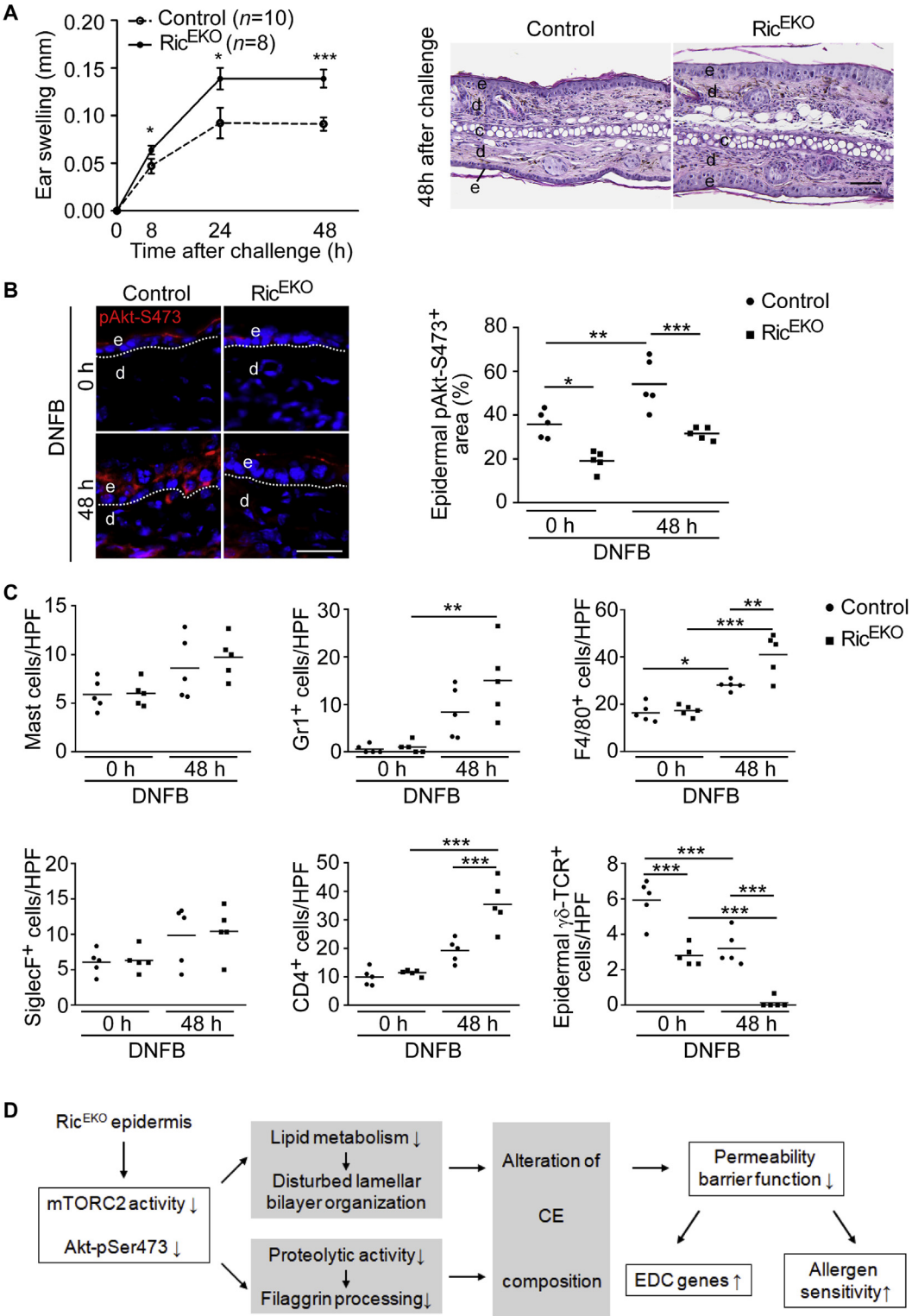

FIG 8. Enhanced percutaneous immune response in Ric^{EKO} mice. **A,** DNFB-induced ACD response. *Right*, Hematoxylin and eosin staining of DNFB-treated ears. *c*, Cartilage; *d*, dermis; *e*, epidermis. **P* < .05 and ****P* < .001. **B,** Phosphorylated Akt-S473 immunofluorescent staining and morphometric quantification of phosphorylated Akt-S473–stained unchallenged (0 hours) and challenged (48 hours) ear skin sections. **C,** Numbers of eosinophils (Siglec-F), mast cells (Giemsa), neutrophils (Gr1), macrophages (F4/80), and T cells (CD4 and γδTCR) per high-power field (*HPF*; ×400 magnification) in unchallenged (0 hours) and challenged (48 hours) ear tissues. **D,** Schematic diagram showing the proposed function of mTORC2 in regulating epidermal barrier function. Each *dot* or *square* represents 1 mouse. Data are presented as means or means ± SEMs. The unpaired *t* test or ANOVA 1-way test with the Bonferroni multiple comparison test was used to calculate *P* values: **P* < .05, ***P* < .01, and ****P* < .001.

controls the multiple molecular factors in epidermal barrier formation is not resolved. Here we propose the Ric^{EKO} mouse as a novel preclinical disease model to advance our incomplete understanding of the molecular regulation of SC assembly and epidermal barrier function.

Ric^{EKO} mice had multiple skin symptoms, which are also hallmarks in patients with compromised epidermal barrier function, including increased SC fragility and increased TEWL.[6] Ric^{EKO} epidermis also showed dysbalanced protease/antiprotease activities combined with attenuated FLG processing, both of which were previously reported to be associated with skin barrier defects in patients.[26,44,54,55] Thus here we identified mTORC2 as a critical regulator of protease-mediated epidermal terminal differentiation.

In addition, a striking feature of *Rictor*-deficient epidermis is disturbed lipid composition. Specifically, we observed quantitative alterations in lipid content and structural alterations in lipid lamellae formation in Ric^{EKO} epidermis. Consistently, expression of multiple genes previously reported to be essential in epidermal lipid synthesis and epidermal function in human subjects were reduced in Ric^{EKO} epidermis, emphasizing the utility of Ric^{EKO} mice as an attractive preclinical disease model for barrier defects.[10,12-15] Recent reports describing a regulatory role for mTORC2 in *de novo* lipid synthesis are limited to hepatic and adipose tissues.[56-58]

Here we provide the first evidence of a role for mTORC2 in epidermal lipid metabolism. However, although it is widely accepted that epidermal lipids are integral components driving the formation and maintenance of the epidermal permeability barrier, the exact mechanistic link how epidermal lipids regulate epidermal barrier function and/or *vice versa*, is not entirely resolved.[59,60] Therefore, although our findings in Ric^{EKO} mice suggest that the quantitative and qualitative perturbations in lipid composition is causative for the observed skin barrier defect in Ric^{EKO} mice, at this stage, we cannot exclude the possibility that perturbed epidermal architecture contributes to perturbed lipid synthesis.[59,60] It will be of interest to investigate in future studies additional downstream mediators of mTORC2 signaling to understand how epidermal *de novo* lipogenesis and SC lipid homeostasis is regulated by mTORC2.

Intriguingly, the number of epidermal DETCs was remarkably reduced in Ric^{EKO} mice. DETC counts are profoundly reduced in patients with AD, as well as in mouse models lacking key SC proteins.[30,61] Consistent with a reduced DETC count in Ric^{EKO} epidermis, expression of several members of *Skint* family genes was downregulated in Rictor-deficient epidermis. *Skint* genes have been identified as essential regulators of DETC cell development.[50] Hence our findings indicate that epidermal mTORC2 activity is critical for anchoring DETCs in the epithelial niche and maintaining the DETC repertoire, potentially mediated through *Skint* genes. However, the reduced epidermal DETC number could be caused by a combination of multiple factors, including attenuated expression of *Skint* genes, perturbed epidermal architecture, and/or disturbed interplay between lipids and/or additional factors and remains to be further investigated in future studies. In addition to the reduced number of epidermal DETCs, the morphology of DETCs was significantly altered in Ric^{EKO} epidermis. DETCs in Ric^{EKO} epidermal sheets lead to a phenotype associated with activation and a protective role in injured epidermis.[50] Thus it is tempting to speculate that DETCs in Ric^{EKO} epidermis compensate for a defective epidermal barrier. Together, our findings suggest an important function of epidermal mTORC2 in maintaining and shaping DETC homeostasis and thus highlight a previously unrecognized function of mTORC2 in the epithelial-immune crosstalk regulating skin barrier function.

Along these lines, increased infiltration of CD4$^+$ T cells and enhanced expression of *Tslp* were also observed in the skin of Ric^{EKO} pups, both of which are hallmarks in the epidermis and keratinocytes of patients with AD.[62] Although adult Ric^{EKO} mouse skin displayed no spontaneous pathologic phenotypes, including skin lesions or signs of skin inflammation, adult mutants exhibited exaggerated percutaneous immune responses. Patients with AD have an increased risk of sensitization to allergens, as well as asthma, rhinitis, and food allergy. Consistently, *FLG* deficiency in mice facilitates and permits increased percutaneous sensitization with protein allergens, irritants, and haptens.[63,64] Collectively, our findings highlight a direct link between epidermal mTORC2 deficiency and paradigmatic symptoms of patients with defective epidermal barrier conditions, such as ichthyosis or AD.

An important question is s follows: What could be the mechanistic explanation for the various processes and symptoms observed in Ric^{EKO} mice? A well-defined function of mTORC2 is phosphorylation of Akt at Ser473, which contributes to Akt-Thr308 phosphorylation by the phosphoinositide-dependent kinase 1, leading to full Akt activation.[20,65] Akt activity is increased at the onset of keratinocyte differentiation and has been shown to regulate epidermal terminal differentiation.[18,24,25] However, the signaling events triggering epidermal Akt activation in epidermal differentiation still remain elusive. We propose a nonredundant role for mTORC2 in Akt-Ser473 activation during epidermal stratification and cornification. It is likely that epidermal mTORC2 acts through Akt in a phosphoinositide-dependent kinase 1–dependent manner because depletion of either component leads to an epidermal barrier phenotype comparable to that in Ric^{EKO} mice.[66,67] Several *in vitro* and *in vivo* studies suggest that proper FLG processing requires Akt activation.[24-26] Accordingly, we observed that Akt-Ser473 phosphorylation was significantly attenuated and that FLG processing was impaired in Ric^{EKO} keratinocytes *in vitro*. Together, our findings suggest that the mTORC2-Akt signaling axis is activated and has mTORC1-independent functions on terminal differentiation to trigger FLG processing and barrier function. Future studies are needed to determine whether induction of epidermal protease activity, lipid metabolism, or both is a direct or indirect downstream target of mTORC2-Akt signaling.

Finally, prenatal Ric^{EKO} epidermis presented a robust upregulation of a stress-response signature characterized by prominent expression of epidermal barrier stress–induced intermediate filament genes, as well as UVB-induced genes. We hypothesize that this induced stress response supports a compensatory protective mechanism in response to the barrier defect, thereby ensuring survival. This hypothesis is further based on the finding that the cytoprotective transcription factor nuclear factor-erythroid 2-related factor 2 *(Nrf2)* and several well-known Nrf2 target genes, including *Krt6, Krt16*, *Sprr2h*, and *S100a*, were all transcriptionally upregulated in Ric^{EKO} epidermis.[68] Along these lines, an Nrf2-regulated compensatory response has been shown to be activated in embryonic epidermis lacking loricrin.[69] Therefore our findings support the idea that the activation of a stress-related homeostasis program is a general feature of a

functionally compromised epidermal barrier. Our discovery that the druggable mTORC2 complex orchestrates this generalized stress response opens interesting avenues for exploring therapeutic boosting of barrier function.

In conclusion, we have demonstrated that postnatal epidermal mTORC2 activity orchestrates epidermal barrier formation and maintenance through regulation of lipid synthesis and FLG processing. We speculate that altered mTORC2 activity might represent another predisposing factor for skin disorders associated with disrupted barrier function. Our findings might be of clinical relevance by, for example, normalizing epidermal mTORC2 activity in patients with defective epidermal barrier conditions by pharmacotherapy.

We thank Michael Piekarek, Gabriele Scherr, and Sebastian Wüst for excellent technical assistance; Dr Stephen M. Sykes (Fox Chase Cancer Center, Philadelphia, Pa) and Dr Kira Gritsman (Department of Medicine, Albert Einstein College of Medicine) for the gift of the myr-AKT plasmid used in this study; Dr Sandra Iden for providing antibodies; Dr Carien Niessen and colleagues in her group for insightful suggestions and technical advice in TEWL measurements; Dr Peter Nürnberg and Dr Janine Altmüller (Cologne Center for Genomics, University of Cologne, Cologne, Germany) for supporting transcriptome and bioinformatic analyses; and the Imaging Facility (CECAD, Cologne University) and Dr Gunter Rappl, (Central Cell Sorting Facility, CMMC, Cologne University) for specialized technical support.

Key messages

- **The Ric^{EKO} mouse had an ichthyosis-like phenotype and might serve as a new preclinical disease model for studying epidermal barrier defects at the molecular level.**
- **Altered mTORC2 activity might represent a predisposing factor for skin disorders associated with disrupted epidermal barrier function.**

REFERENCES

1. Elias PM. Skin barrier function. Curr Allergy Asthma Rep 2008;8:299-305.
2. Kubo A, Nagao K, Amagai M. Epidermal barrier dysfunction and cutaneous sensitization in atopic diseases. J Clin Invest 2012;122:440-7.
3. Duff M, Demidova O, Blackburn S, Shubrook J. Cutaneous manifestations of diabetes mellitus. Clin Diabetes 2015;33:40-8.
4. Boireau-Adamezyk E, Baillet-Guffroy A, Stamatas GN. Age-dependent changes in stratum corneum barrier function. Skin Res Technol 2014;20:409-15.
5. Craiglow BG. Ichthyosis in the newborn. Semin Perinatol 2013;37:26-31.
6. Candi E, Schmidt R, Melino G. The cornified envelope: a model of cell death in the skin. Nat Rev Mol Cell Biol 2005;6:328-40.
7. Lopez-Pajares V, Yan K, Zarnegar BJ, Jameson KL, Khavari PA. Genetic pathways in disorders of epidermal differentiation. Trends Genet 2013;29:31-40.
8. Smith FJD, Irvine AD, Terron-Kwiatkowski A, Sandilands A, Campbell LE, Zhao YW, et al. Loss-of-function mutations in the gene encoding filaggrin cause ichthyosis vulgaris. Nat Genet 2006;38:337-42.
9. Sandilands A, Sutherland C, Irvine AD, McLean WH. Filaggrin in the frontline: role in skin barrier function and disease. J Cell Sci 2009;122:1285-94.
10. Brunner PM, Israel A, Zhang N, Leonard A, Wen HC, Huynh T, et al. Early-onset pediatric atopic dermatitis is characterized by T(H)2/T(H)17/T(H)22-centered inflammation and lipid alterations. J Allergy Clin Immunol 2018;141:2094-106.
11. Gruber R, Elias PM, Crumrine D, Lin TK, Brandner JM, Hachem JP, et al. Filaggrin genotype in ichthyosis vulgaris predicts abnormalities in epidermal structure and function. Am J Pathol 2011;178:2252-63.
12. Vasireddy V, Uchida Y, Salem N, Kim SY, Mandal MNA, Reddy GB, et al. Loss of functional ELOVL4 depletes very long-chain fatty acids (>= C28) and the unique omega-O-acylceramides in skin leading to neonatal death. Hum Mol Genet 2007;16:471-82.
13. Westerberg R, Tvrdik P, Unden AB, Mansson JE, Norlen L, Jakobsson A, et al. Role for ELOVL3 and fatty acid chain length in development of hair and skin function. J Biol Chem 2004;279:5621-9.
14. Aldahmesh MA, Mohamed JY, Alkuraya HS, Verma IC, Puri RD, Alaiya AA, et al. Recessive mutations in ELOVL4 cause ichthyosis, intellectual disability, and spastic quadriplegia. Am J Hum Genet 2011;89:745-50.
15. Ilic D, Bollinger JM, Gelb M, Mauro TM. sPLA2 and the epidermal barrier. Biochim Biophys Acta 2014;1841:416-21.
16. Natsuga K. Epidermal barriers. Cold Spring Harb Perspect Med 2014;4:a018218.
17. Blanpain C, Fuchs E. Epidermal homeostasis: a balancing act of stem cells in the skin. Nat Rev Mol Cell Biol 2009;10:207-17.
18. Ding X, Bloch W, Iden S, Ruegg MA, Hall MN, Leptin M, et al. mTORC1 and mTORC2 regulate skin morphogenesis and epidermal barrier formation. Nat Commun 2016;7:13226.
19. Kakanj P, Moussian B, Gronke S, Bustos V, Eming SA, Partridge L, et al. Insulin and TOR signal in parallel through FOXO and S6K to promote epithelial wound healing. Nat Commun 2016;7:12972.
20. Saxton RA, Sabatini DM. mTOR signaling in growth, metabolism, and disease. Cell 2017;168:960-76.
21. Wullschleger S, Loewith R, Hall MN. TOR signaling in growth and metabolism. Cell 2006;124:471-84.
22. Sarbassov DD, Ali SM, Sengupta S, Sheen JH, Hsu PP, Bagley AF, et al. Prolonged rapamycin treatment inhibits mTORC2 assembly and Akt/PKB. Mol Cell 2006;22:159-68.
23. Jacinto E, Loewith R, Schmidt A, Lin S, Ruegg MA, Hall A, et al. Mammalian TOR complex 2 controls the actin cytoskeleton and is rapamycin insensitive. Nat Cell Biol 2004;6:1122-8.
24. Calautti E, Li J, Saoncella S, Brissette JL, Goetinck PF. Phosphoinositide 3-kinase signaling to Akt promotes keratinocyte differentiation versus death. J Biol Chem 2005;280:32856-65.
25. O'Shaughnessy RF, Welti JC, Cooke JC, Avilion AA, Monks B, Birnbaum MJ, et al. AKT-dependent HspB1 (Hsp27) activity in epidermal differentiation. J Biol Chem 2007;282:17297-305.
26. Naeem AS, Tommasi C, Cole C, Brown SJ, Zhu Y, Way B, et al. A mechanistic target of rapamycin complex 1/2 (mTORC1)/V-Akt murine thymoma viral oncogene homolog 1 (AKT1)/cathepsin H axis controls filaggrin expression and processing in skin, a novel mechanism for skin barrier disruption in patients with atopic dermatitis. J Allergy Clin Immunol 2016;139:1228-41.
27. Ding X, Lucas T, Marcuzzi GP, Pfister H, Eming SA. Distinct functions of epidermal and myeloid-derived VEGF-A in skin tumorigenesis mediated by HPV8. Cancer Res 2015;75:330-43.
28. Knipper JA, Willenborg S, Brinckmann J, Bloch W, Maass T, Wagener R, et al. Interleukin-4 receptor alpha signaling in myeloid cells controls collagen fibril assembly in skin repair. Immunity 2015;43:803-16.
29. Subramanian A, Tamayo P, Mootha VK, Mukherjee S, Ebert BL, Gillette MA, et al. Gene set enrichment analysis: a knowledge-based approach for interpreting genome-wide expression profiles. Proc Natl Acad Sci U S A 2005;102:15545-50.
30. Sevilla LM, Nachat R, Groot KR, Klement JF, Uitto J, Djian P, et al. Mice deficient in involucrin, envoplakin, and periplakin have a defective epidermal barrier. J Cell Biol 2007;179:1599-612.
31. Reichelt J, Breiden B, Sandhoff K, Magin TM. Loss of keratin 10 is accompanied by increased sebocyte proliferation and differentiation. Eur J Cell Biol 2004;83:747-59.
32. Signorelli P, Hannun YA. Analysis and quantitation of ceramide. Methods Enzymol 2002;345:275-94.
33. Belgardt BF, Mauer J, Wunderlich FT, Ernst MB, Pal M, Spohn G, et al. Hypothalamic and pituitary c-Jun N-terminal kinase 1 signaling coordinately regulates glucose metabolism. Proc Natl Acad Sci U S A 2010;107:6028-33.
34. Kharas MG, Okabe R, Ganis JJ, Gozo M, Khandan T, Paktinat M, et al. Constitutively active AKT depletes hematopoietic stem cells and induces leukemia in mice. Blood 2010;115:1406-15.
35. Ding X, Wang X, Sontag S, Qin J, Wanek P, Lin Q, et al. The polycomb protein Ezh2 impacts on induced pluripotent stem cell generation. Stem Cells Dev 2014;23:931-40.
36. Bentzinger CF, Romanino K, Cloetta D, Lin S, Mascarenhas JB, Oliveri F, et al. Skeletal muscle-specific ablation of raptor, but not of rictor, causes metabolic changes and results in muscle dystrophy. Cell Metab 2008;8:411-24.
37. Hafner M, Wenk J, Nenci A, Pasparakis M, Scharffetter-Kochanek K, Smyth N, et al. Keratin 14 Cre transgenic mice authenticate keratin 14 as an oocyte-expressed protein. Genesis 2004;38:176-81.
38. Mischke D, Korge BP, Marenholz I, Volz A, Ziegler A. Genes encoding structural proteins of epidermal cornification and S100 calcium-binding proteins form a gene complex ("epidermal differentiation complex") on human chromosome 1q21. J Invest Dermatol 1996;106:989-92.

39. Lessard JC, Pina-Paz S, Rotty JD, Hickerson RP, Kaspar RL, Balmain A, et al. Keratin 16 regulates innate immunity in response to epidermal barrier breach. Proc Natl Acad Sci U S A 2013;110:19537-42.
40. Enk CD, Jacob-Hirsch J, Gal H, Verbovetski I, Amariglio N, Mevorach D, et al. The UVB-induced gene expression profile of human epidermis in vivo is different from that of cultured keratinocytes. Oncogene 2006;25:2601-14.
41. Elias PM, Williams ML, Holleran WM, Jiang YJ, Schmuth M. Pathogenesis of permeability barrier abnormalities in the ichthyoses: inherited disorders of lipid metabolism. J Lipid Res 2008;49:697-714.
42. Breiden B, Sandhoff K. The role of sphingolipid metabolism in cutaneous permeability barrier formation. Biochim Biophys Acta 2014;1841:441-52.
43. Ovaere P, Lippens S, Vandenabeele P, Declercq W. The emerging roles of serine protease cascades in the epidermis. Trends Biochem Sci 2009;34:453-63.
44. Egberts F, Heinrich M, Jensen JM, Winoto-Morbach S, Pfeiffer S, Wickel M, et al. Cathepsin D is involved in the regulation of transglutaminase 1 and epidermal differentiation. J Cell Sci 2004;117:2295-307.
45. Oji V, Oji ME, Adamini N, Walker T, Aufenvenne K, Raghunath M, et al. Plasminogen activator inhibitor-2 is expressed in different types of congenital ichthyosis: in vivo evidence for its cross-linking into the cornified cell envelope by transglutaminase-1. Br J Dermatol 2006;154:860-7.
46. Yuspa SH, Kilkenny AE, Steinert PM, Roop DR. Expression of murine epidermal differentiation markers is tightly regulated by restricted extracellular calcium concentrations in vitro. J Cell Biol 1989;109:1207-17.
47. Tu CL, Crumrine DA, Man MQ, Chang WH, Elalieh H, You M, et al. Ablation of the calcium-sensing receptor in keratinocytes impairs epidermal differentiation and barrier function. J Invest Dermatol 2012;132:2350-9.
48. Elias PM. Therapeutic implications of a barrier-based pathogenesis of atopic dermatitis. Ann Dermatol 2010;22:245-54.
49. Komori H, Meehar TF, Havran WL. Epithelial and mucosal gamma delta T cells. Curr Opin Immunol 2006;18:534-8.
50. Nielsen MM, Witherden DA, Havran WL. γδ T cells in homeostasis and host defence of epithelial barrier tissues. Nat Rev Immunol 2017;17:733-45.
51. Barbee SD, Woodward MJ, Turchinovich G, Mention JJ, Lewis JM, Boyden LM, et al. Skint-1 is a highly specific, unique selecting component for epidermal T cells. Proc Natl Acad Sci U S A 2011;108:3330-5.
52. De Benedetto A, Kubo A, Beck LA. Skin barrier disruption: a requirement for allergen sensitization? J Invest Dermatol 2012;132:949-63.
53. Weidinger S, Novak N. Atopic dermatitis. Lancet 2016;387:1109-22.
54. Toomes C, James J, Wood AJ, Wu CL, McCormick D, Lench N, et al. Loss-of-function mutations in the cathepsin C gene result in periodontal disease and palmoplantar keratosis. Nat Genet 1999;23:421-4.
55. Cheng T, Hitomi K, van Vlijmen-Willems IMJJ, de Jongh GJ, Yamamoto K, Nishi K, et al. Cystatin M/E is a high affinity inhibitor of cathepsin V and cathepsin L by a reactive site that is distinct from the legumain-binding site—a novel clue for the role of cystatin M/E in epidermal cornification. J Biol Chem 2006;281:15893-9.
56. Caron A, Richard D, Laplante M. The roles of mTOR complexes in lipid metabolism. Annu Rev Nutr 2015;35:321-48.
57. Guri Y, Colombi M, Dazert E, Hindupur SK, Roszik J, Moes S, et al. mTORC2 promotes tumorigenesis via lipid synthesis. Cancer Cell 2017;32:807-23.
58. Hagiwara A, Cornu M, Cybulski N, Polak P, Betz C, Trapani F, et al. Hepatic mTORC2 activates glycolysis and lipogenesis through Akt, glucokinase, and SREBP1c. Cell Metab 2012;15:725-38.
59. van Smeden J, Janssens M, Gooris GS, Bouwstra JA. The important role of stratum corneum lipids for the cutaneous barrier function. Biochim Biophys Acta 2014;1841:295-313.
60. Bhattacharya N, Sato WJ, Kelly A, Ganguli-Indra G, Indra AK. Epidermal lipids: key mediators of atopic dermatitis pathogenesis. Trends Mol Med 2019;25:551-62.
61. Katsuta M, Takigawa Y, Kimishima M, Inaoka M, Takahashi R, Shiohara T. NK cells and gamma delta(+) T cells are phenotypically and functionally defective due to preferential apoptosis in patients with atopic dermatitis. J Immunol 2006;176:7736-44.
62. Ziegler SF, Artis D. Sensing the outside world: TSLP regulates barrier immunity. Nat Immunol 2010;11:289-93.
63. Kawasaki H, Nagao K, Kubo A, Hata T, Shimizu A, Mizuno H, et al. Altered stratum corneum barrier and enhanced percutaneous immune responses in filaggrin-null mice. J Allergy Clin Immunol 2012;129:1538-46.
64. Fallon PG, Sasaki T, Sandilands A, Campbell LE, Saunders SP, Mangan NE, et al. A homozygous frameshift mutation in the mouse Flg gene facilitates enhanced percutaneous allergen priming. Nat Genet 2009;41:602-8.
65. Sarbassov DD, Guertin DA, Ali SM, Sabatini DM. Phosphorylation and regulation of Akt/PKB by the rictor-mTOR complex. Science 2005;307:1098-101.
66. Dainichi T, Hayden MS, Park SG, Oh H, Seeley JJ, Grinberg-Bleyer Y, et al. PDK1 is a regulator of epidermal differentiation that activates and organizes asymmetric cell division. Cell Rep 2016;15:1615-23.
67. Peng XD, Xu PZ, Chen ML, Hahn-Windgassen A, Skeen J, Jacobs J, et al. Dwarfism, impaired skin development, skeletal muscle atrophy, delayed bone development, and impeded adipogenesis in mice lacking Akt1 and Akt2. Genes Dev 2003;17:1352-65.
68. Schafer M, Farwanah H, Willrodt AH, Huebner AJ, Sandhoff K, Roop D, et al. Nrf2 links epidermal barrier function with antioxidant defense. EMBO Mol Med 2012;4:364-79.
69. Huebner AJ, Dai D, Morasso M, Schmidt EE, Schafer M, Werner S, et al. Amniotic fluid activates the nrf2/keap1 pathway to repair an epidermal barrier defect in utero. Dev Cell 2012;23:1238-46.

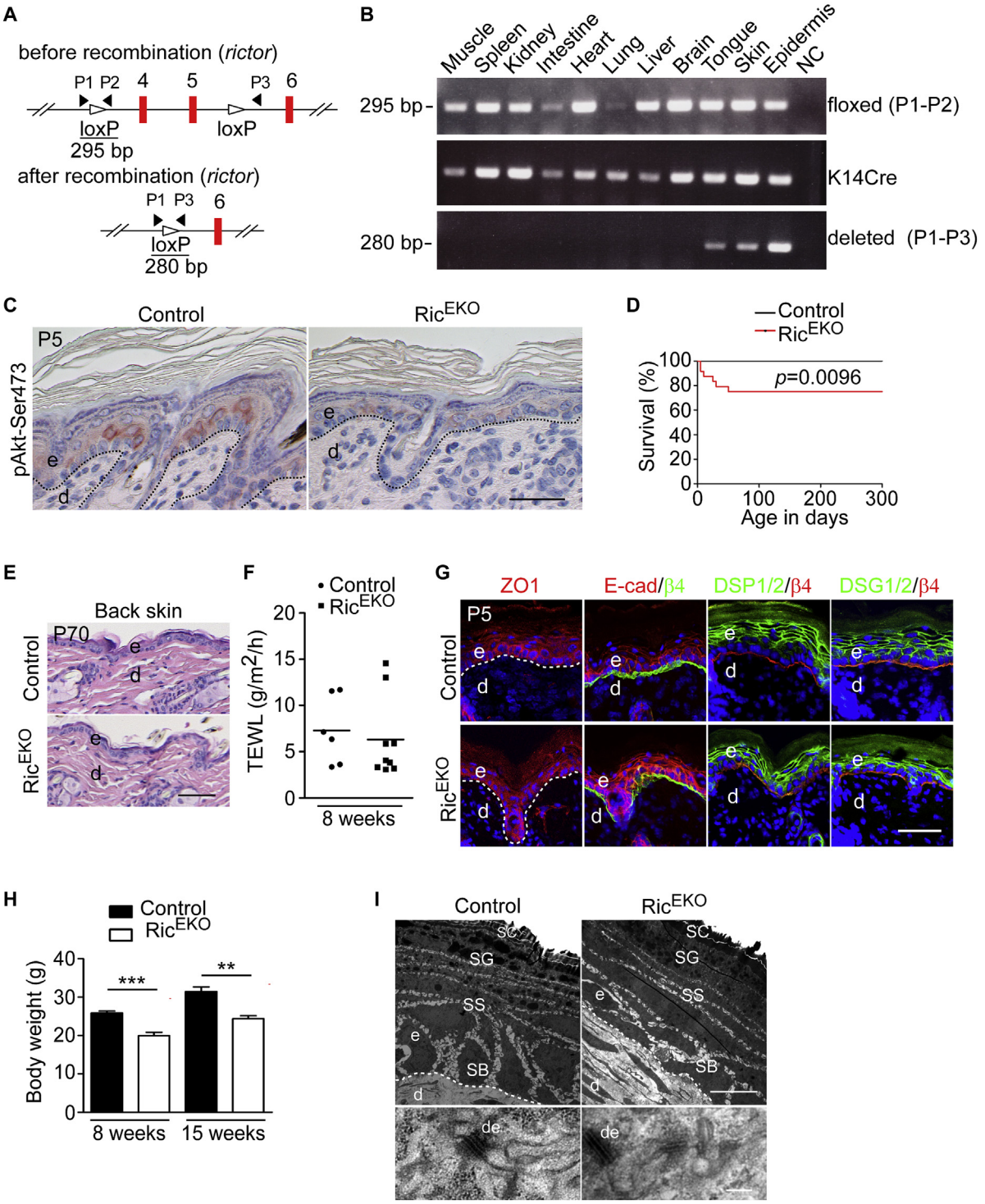

FIG E1. Conditional targeting of the *Rictor* gene in epidermal keratinocytes. **A,** Scheme illustrating the *Rictor* gene construct, the 2 loxP sites flanking exons, and the PCR fragment length before and after recombination. **B,** PCR product of genomic DNA isolated from various tissues. **C,** Phosphorylated Akt (Akt-pS473) immunostaining of back skin of control and Ric^{EKO} mice at P5. *Scale bar* = 25 μm. **D,** Survival curve of control (n = 16) and Ric^{EKO} (n = 15) mice. The Mantel-Cox test was used to calculate *P* values. **E,** Representative hematoxylin and eosin–stained back skin sections from control and Ric^{EKO} mice at P70. *Scale bar* = 25 μm. **F,** TEWL in Ric^{EKO} and control mice. **G,** Representative immunofluorescence staining at P5 for zonula occludens 1 *(ZO1)*, E-cadherin *(E-cad)*, desmoplakin 1/2 *(DSP1/2)*, desmoglein 1/2 *(DSG1/2)*, and β_4-integrin (red). *White dashed lines* indicate basement membrane. Nuclei are visualized with 4′,6-diamidino-2-phenylindole (blue). *Scale bar* = 20 μm. **H,** Body weight of control (n = 8) and Ric^{EKO} (n = 7) mice at different ages. **I,** Ultrastructural analysis of back skin epidermis of control and Ric^{EKO} mice at P5. *Lower panel*, Higher magnification images show desmosome *(de)* structure. *d*, Dermis; *e*, epidermis; *SB*, stratum basale; *SS*, stratum spinosum. *Scale bar* = 5 μm *(upper panel)* and 100 nm *(lower panel)*. Each *dot* or *square* represents 1 mouse. Data are presented as means or as means ± SEMs. The unpaired *t* test was used to calculate *P* values: $^{**}P < .01$ and $^{***}P < .001$.

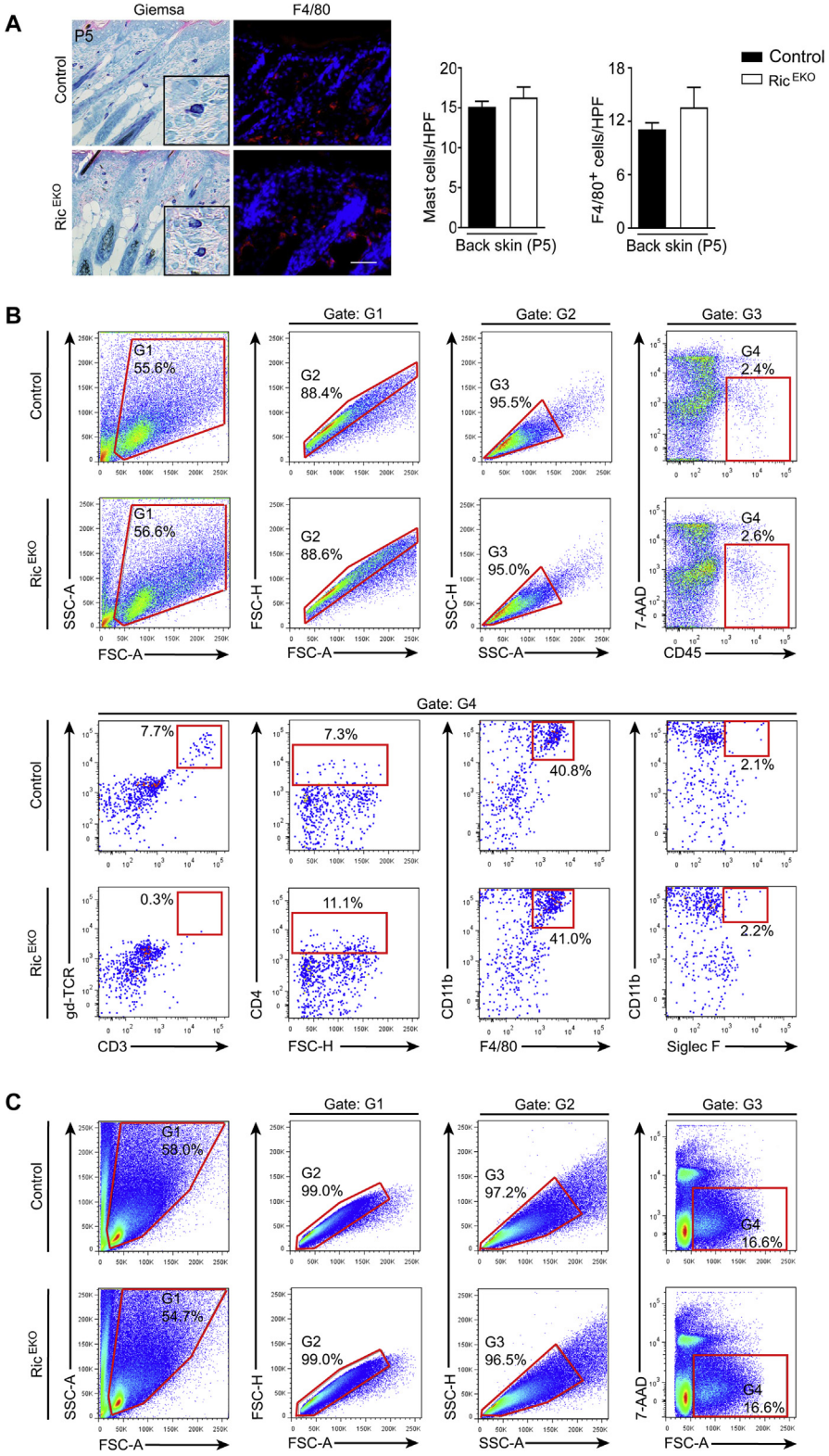

FIG E2. Immune cell composition and gating strategies for FACS analysis of cell suspensions isolated from back skin and ear. **A,** *Left*, Representative Giemsa staining and F4/80 immunostaining with back skin sections from control and Ric^{EKO} mice at P5. *Right*, Quantification of mast cells and F4/80^{+} macrophage cells per high-power field (*HPF*; n = 5 per genotype). *Scale bar* = 25 μm. Data are presented as means ± SEMs. **B,** Representative FACS analysis of single-cell suspensions of back skin in control and Ric^{EKO} mice (P5). *Upper panel*, Single cells were gated (G1-3) and analyzed for 7-AAD staining and expression of CD45 (G4). *Lower panel*, 7-AAD^{-}CD45^{+} cells (G4) were analyzed for expression of (from left to right) CD3 and γδTCR, CD4, CD11b and F4/80, and CD11b and Siglec-F. **C,** Representative FACS analysis of single-cell suspensions of ear skin in control and Ric^{EKO} mice (P70). Single cells (G1-3) and 7-AAD^{-} cells (G4) were gated. *Red polygons* indicate the gate, and percentages indicate the proportion of gated cells. *FSC-A*, Forward scatter area; *FSC-H*, forward scatter height; *G*, gate; *SSC-A*, sideward scatter area; *SSC-H*, sideward scatter height.

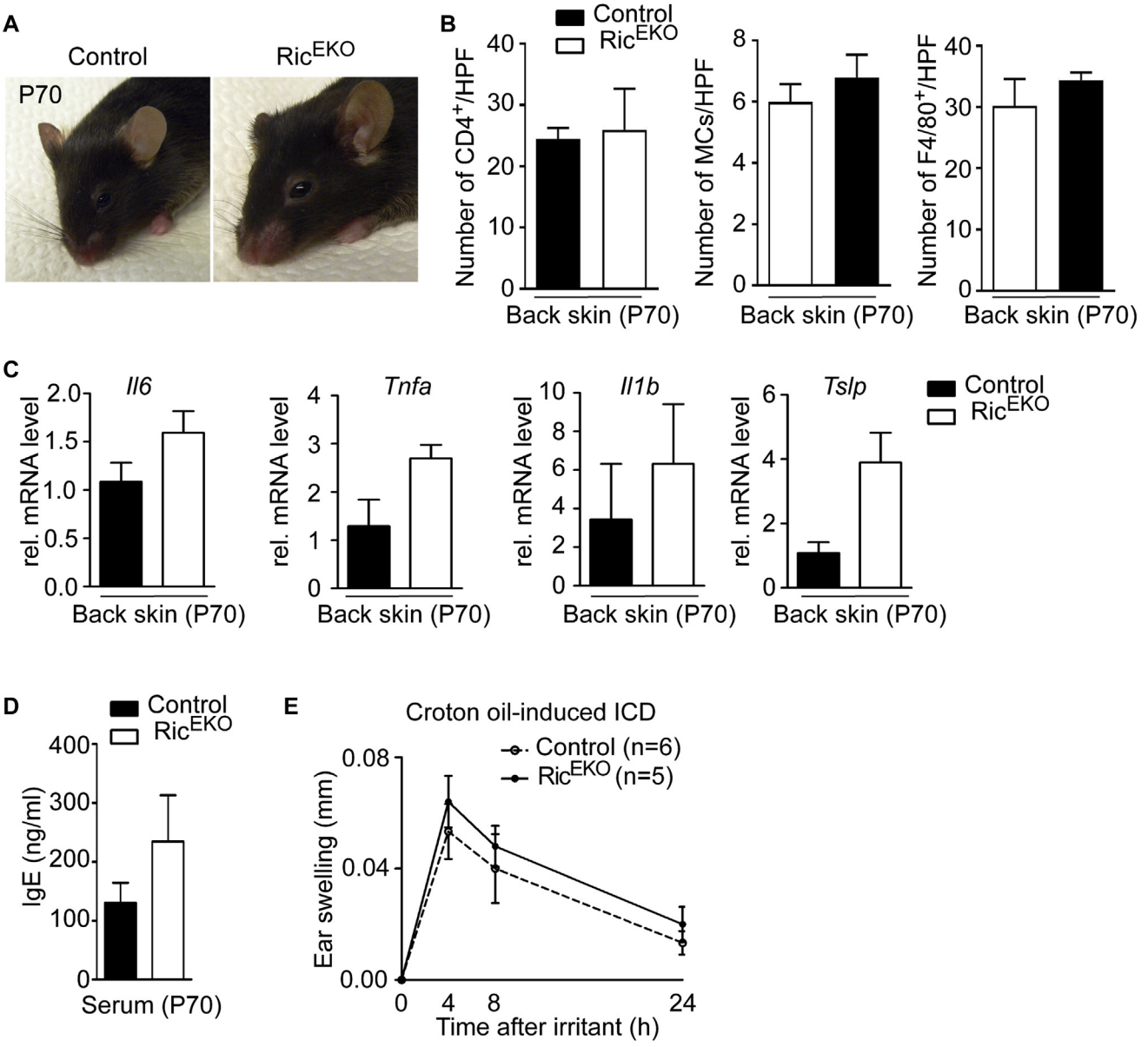

FIG E3. Mild skin inflammation in naive Ric^{EKO} mice under specific pathogen-free conditions. **A,** Representative macroscopic appearance of control and Ric^{EKO} mice at P70. **B,** Quantification of CD4^{+} cells, mast cells *(MCs)*, and F4/80^{+} macrophages in back skin sections from control and Ric^{EKO} mice at P70 (n = 5 per genotype). *HPF*, High-power field. **C,** qRT-PCR analysis of *Il6*, *Tnfα*, *Il1b*, and *Tslp* expression in Ric^{EKO} and control skin at P70 (n = 5 per genotype). **D,** Serum IgE amounts in Ric^{EKO} and control mice were determined by using ELISA (n = 6 per genotype) at P70. **E,** Croton oil–induced ICD response. Ear swelling of control and Ric^{EKO} animals after topical application of croton oil was calculated and shown (n = 5 per genotype). Data are presented as means ± SEMs.

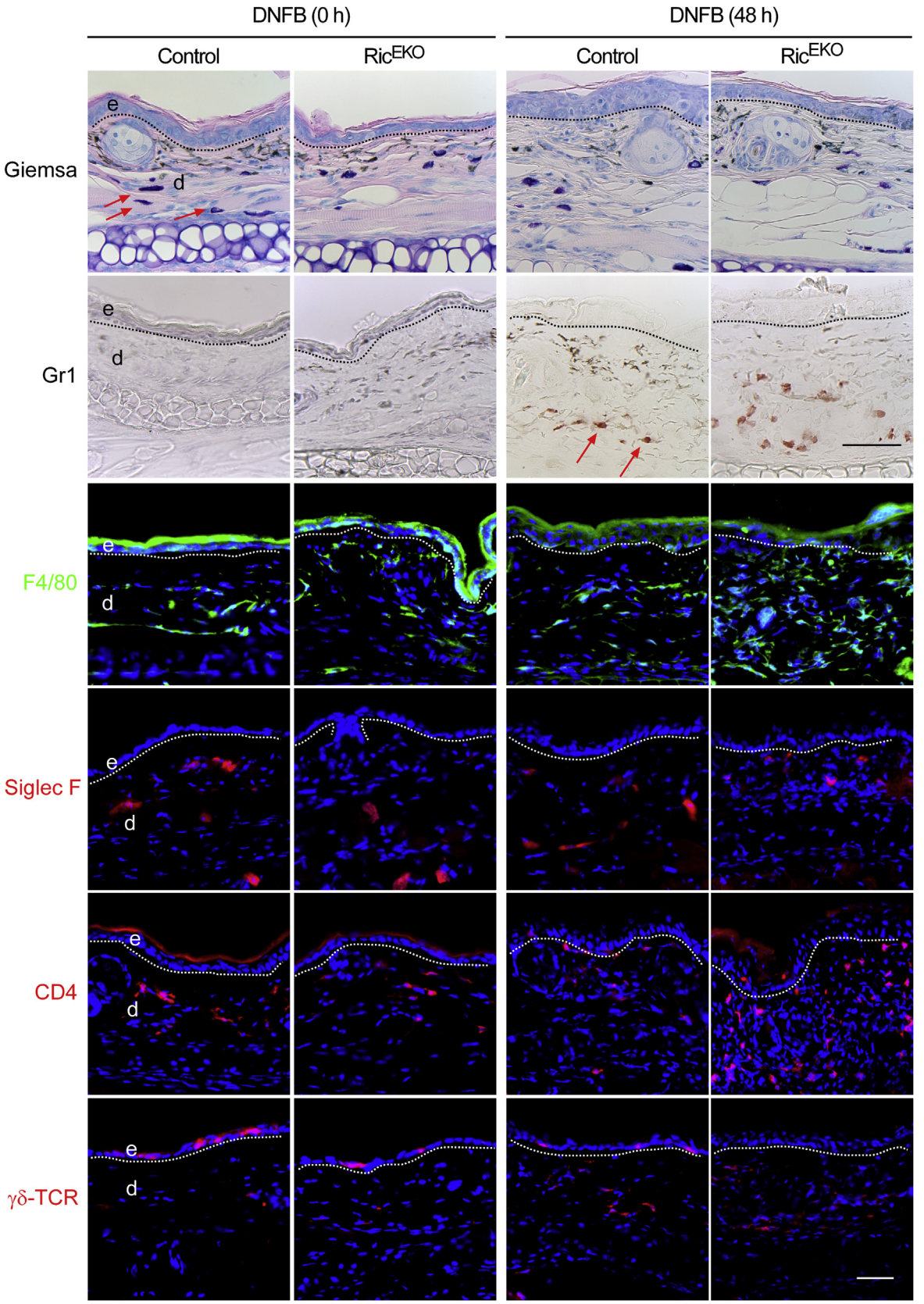

FIG E4. Immune cell infiltration in ear skin tissue. Representative Giemsa staining and immunohistochemical staining for Gr1, F4/80, Siglec-F, CD4, and γδTCR of untreated (DNFB, 0 hours) and treated (DNFB, 48 hours) ear sections from control and Ric^{EKO} mice (n = 5). *Arrows* indicate mast cells (Giemsa stain, purple) or polymorphonuclear cells (Gr1 stain, brown), and *dashed lines* indicate the border between the epidermis and dermis. *d*, Dermis; *e*, epidermis. *Scale bar* = 25 μm.

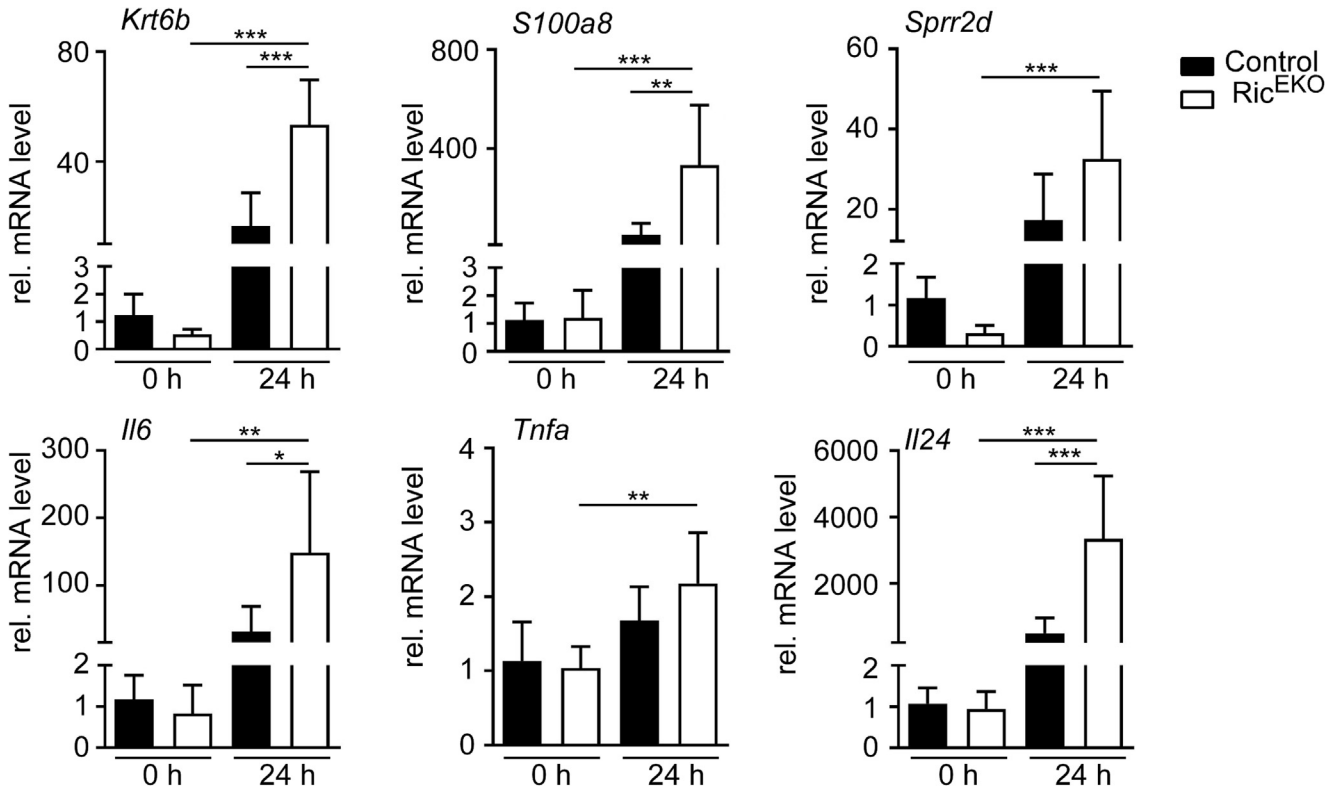

FIG E5. Gene expression analysis in ear skin tissue. qRT-PCR analysis of stress response gene (*Krt6b*, *S100a8*, and *Sprr2d*) and inflammatory mediator (*Il6*, *Tnfa*, and *Il24*) expression in untreated (DNFB, 0 hours) and treated (DNFB, 24 hours) ear skin tissues from control and Ric^{EKO} mice (n = 6 per genotype). Gene expression in untreated control ear skin was referred as 1, and relative fold changes were analyzed and shown. Data are presented as means ± SEMs. One-way ANOVA with the Bonferroni multiple comparison test was used. $*P < .05$, $**P < .01$, and $***P < .001$.

TABLE E1. Antibodies used for immunostaining and Western blotting

Name	Catalog no.	Source
Primary antibodies used for immunostaining		
Akt-pS473	9271	Cell Signaling, Beverly, Mass
CD4	14-0042-85	Thermo Fisher Scientific, Waltham, Mass
Ly-6G and Ly-6C (Gr1)	550291	BD Biosciences, San Jose, Calif
Siglec-F	552126	BD Biosciences
CD3	MCA1477	AbD Serotec, Kidlington, United Kingdom
F4/80	MOF4F (V500)	Dianova, New York, NY
ZO-1	(Hybridoma) rat, clone R26.4C	
Desmoglein 1/2	61002	Progen, Heidelberg, Germany
Desmoplakin 1/2	61003	Progen
β_4-Integrin	555719	BD Biosciences, San Jose, Calif
E-cadherin	610182	BD Biosciences
γδTCR	553175	BD Biosciences
Secondary antibodies used for immunostaining		
Anti-rabbit IgG Alexa Fluor 488	A-32731	Thermo Fisher Scientific
Anti-rabbit IgG Alexa Fluor 568	A-11011	Thermo Fisher Scientific
Anti-rat IgG Alexa Fluor 488	A-11006	Thermo Fisher Scientific
Anti-mouse Alexa Fluor 594	A-11032	Thermo Fisher Scientific
Anti-rabbit IgG HRP	K4003	DAKO, Glostrup, Denmark
Primary antibodies used for Western blotting		
S6-pS240/244	5364	Cell Signaling
Rictor	2140	Cell Signaling
Akt-pS473	9271	Cell Signaling
Loricrin	PRB-145P	Covance, Princeton, NJ
FLG	PRB-417P	Covance
Akt	9272	Cell Signaling
Keratin 10	PRB-159P	Covance
β-Actin (C4)	MAB1501	Sigma-Aldrich, St Louis, Mo
α-Tubulin (B-5-1-2)	T6074	Sigma-Aldrich
Secondary antibodies used for Western blotting		
Anti-rabbit IgG-HRP	P0448	DAKO
Anti-mouse IgG-HRP	P0161	DAKO

HRP, Horseradish peroxidase; *ZO-1*, zonula occludens 1.

TABLE E2. Primer sequence used for qRT-PCR analysis

Gene	Forward primer	Reverse primer
Gapdh	CATGTTTGTGATGGGTGTGA	AATGCCAAAGTTGTCATGGA
Nrf2	CCATTCCCGAATTACAGTGTCTTA	CGCCAAAATCTGTGTTTAAGGTG
Sfn	CCGAACGGTATGAAGACATGG	CGGTACTTTCACCTCGGG
Slc7a11	CAACAAAGATCGGGACTGCT	GCTGGCTGGTTTTACCTCAA
Srxn1	CGGTGCACAACGTACCAAT	TTGATCCAGAGGACGTCGAT
Sprr2d	CTGGTACTCAAGGCCGAGAC	CAGGGCACTTTGGTGGAG
Sprr2e	CAGGTCCTAGGCTACTTTGGAG	ACTGTGGATGAGGACAAGGC
Sprr2h	GACACTTGGTACTCAAGCTCTGG	TGCACTGCTGCTGTTGGTAA
Rptn	TCCTGCCTCTTCTGCTCATT	AGCGCCTACCCCATGATATT
Lce3f	TCCTGGCTCTTCCTGTTCTC	CCCAGGCAGTTATCAAAAGC
S100a8	GCCGTCTGAACTGGAGAAG	GTGAGATGCCACACCCACTT
Keratin6b	TGCAGACGAGATCAACTTCC	TGCAGACGAGATCAACTTCC
Elovl3	CTGTTGCTCATCGTTGTTGG	GCTTGAGGCCCACTGTAAAC
Pla2g5	CTCACACTGGCTTGGTTCCT	CATAACAACGGTCGTGCATC
Ctsh	CACGGAGACGGAGTTACCAG	GTGGCCATTACACTCCTGCT
Ctsd	AATCCCTCTGCGCAAGTTCA	CACTGGCTCCGTGGTCTTAG
Slpi	CGGCAAATACAAGTGCTGTG	CCTGGGAGCAGGGAAGTAGT
Serpinb2	TGCCAGCTTTCCAAGAAGCATT	AGATTGAGGGCAAACATGGTG
Rictor	GAGAAAGCTGGGCCATCTGA	AACCCGGCTGCTCTTACTTC
Tslp	TCTCAGGAGCCTCTTCATCCT	CTCACAGTCCTCGATTTGCTC
Il1α	GTCGGGAGGAGACGACTCTA	TGGTCACAAACAGTGGGAGG
Il1β	GGACCCCAAAAGATGAAGGGCTGC	GCTCTTGTTGATGTGCTGCTGCG
Il24	TGCCAAGTGACAGGGGTGGTTCT	CAGCACCCGAGACATTCCGCAG
Il33	TGATCAAAGAGGCCGGGAAC	ACGCAGATTCCGCCTTTACA
Ccl2	TCCACGTGTTGGCTCAGCCAG	CCAGCCTACTCATTGGGATCATCTT
Tnfa	GACCCTCACACTCAGATCATCTTCT	CCTCCACTTGGTGGTTTGCT

TABLE E3. Differentially expressed genes in Gene Ontology term analysis identified biological processes (related to Fig 3)

Biological processes	
Upregulated genes in Ric^{EKO} epidermis	
Peptide cross-linking	*LCE3A, LCE3B, LCE3C, COL3A1, LCE3D, SPRR2H, SPRR2F, SPRR2E, SPRR2K, SPRR2I, LCE1J, SPRR2D, SPRR1A, SPRR2A3, SPRR1B, SPRR2B, TGM1, SPRR2A2, SPRR3, LCE3F, LCE3E, THBS1, LCE1K*
Keratinization	*KRT6A, KRT6B, SPRR2H, SPRR2F, SFN, SPRR2E, SPRR2K, SPRR2I, KRT17, KRT16, SPRR2D, SPRR1A, SPRR2A3, SPRR1B, CNFN, SPRR2B, TGM1, SPRR2A2, SPRR3*
Keratinocyte differentiation	*PTGS2, LCE3A, LCE3B, LCE3C, LCE3D, SPRR2H, SPRR2F, SFN, SPRR2E, SPRR2K, SPRR2I, LCE1J, KRT16, SPRR2D, SPRR1A, SPRR2A3, SPRR1B, SPRR2B, TGM1, SPRR2A2, SPRR3, LCE3F, LCE3E, LCE1K*
Wound healing	*DCBLD2, KRT6A, NOG, S100A8, TNC, COL3A1, CXCL2, TGFBR2, IL24, ELK3, AQP1, TPM1, MMP12, TIMP1, MACF1, CCL20, SERPINE1, SERPINB2, TGFA, CNN2, LOX, COL1A1, NBEAL2*
Cell adhesion	*CADM4, VCL, NOV, CGREF1, COL12A1, CYR61, KIRREL3, BYSL, CDHR1, ADGRE5, FBLIM1, THY1, TNFAIP6, BVES, HAS1, VCAN, LAMC2, MFAP4, TNFRSF12A, TNC, ITGB4, ITGB1, DCHS1, PTK2B, ITGB6, COL6A2, COL6A1, THBS1, THBS2, THBS3, DPT, COL18A1, PODXL, ITGA3, TINAGL1, PCDH17, COL5A1, LYVE1, COL19A1, CASS4, ITGA6, ITGA5, DSG3, PKP4, ITGA7, SULF1, DSC2, ABL2, NTM, MYH10*
Downregulated genes in Ric^{EKO} epidermis	
Immune system process	LY86, TLR1, LY9, C1QC, SKAP1, ISG20, TLR9, OASL2, OASL1, CLEC4A2, CD300C2, CD3E, PRG2, PIK3CD, PADI4, TRAT1, CD84, C1QA, C1QB, H2-AA, CD300LF, TXK, RNF135, TNFAIP8L2, KLRK1, UNC93B1, SP110, OAS2, IL34, RNF125, NAIP5, PSTPIP1, ZAP70, MR1, CSF1R, CD7, ZBP1, ITK, CARD9, THEMIS, HCK, TNFRSF13C, CTLA4, TRIL, FCGR1, PSMB9, IFIT3, LAT, IFIT2, H2-EB1, C1RL, THEMIS2
Lipid metabolic process	ACOX2, PPARA, ALOX12E, HINT2, BSCL2, 4833423E24RIK, GPCPD1, ACOX3, FAR2, INSIG2, APOE, ELOVL3, NPC1L1, CES1D, FA2H, PLD4, DECR1, LPCAT2, PNPLA5, HSD11B1, NEU3, THEM5, AKR1D1, PLA2G5, HACL1, ECH1, HSD17B2, ABHD3, CERS4, ACSBG1, PLIN5, ACSL4, ACAA1B, GAL3ST1, ACSL6, SCD1, SOAT1, PLA2G16, SCD3, A4GALT, PLB1, CYP46A1, ACER2, ACER1, FADS3, SPTSSB, FAM213B, ACACB, CRAT, FADS6, GDPD1, AWAT2, ACSM3, AWAT1, ACSM2, ACSM1, LIPC
Metabolic process	ACOX2, ARSB, ALAD, ARSG, HEXB, ECHDC1, GM436, ACOX3, UGT1A7C, UGT1A6B, PHOSPHO1, 9430007A20RIK, ACOXL, NEIL2, FBP1, ALDH3B2, LPCAT2, UGT1A1, PNPLA5, AADAC, CAMK1, NEU3, ALPL, ECH1, GM5538, ISOC2B, HSD3B6, UGT3A1, UGT3A2, ACSBG1, C130079G13RIK, ALDH1A1, ALDH1A7, ACSL4, ACAA1B, FAHD2A, ACSL6, GSTA2, GSTA3, ACY3, PM20D1, NPL, GM13124, ACACB, ENGASE, CPS1, ACSM3, ACSM2, ACSM1, LYG2, ARSA, GM13178, GM13177, ACAD10
Fatty acid metabolic process	ACOX2, PPARA, ECH1, ALOX12E, 4833423E24RIK, ACSBG1, ACOX3, CRYL1, ELOVL3, ACSL4, ACAA1B, ACSL6, SCD1, SCD3, ACOXL, FA2H, FADS3, FAM213B, ACACB, DECR1, CRAT, FADS6, ACSM3, ACSM2, ACSM1, LIPC, THEM5
Innate immune response	TNFAIP8L2, LY86, TLR1, KLRK1, UNC93B1, SP110, TRIM15, OAS2, LY9, IL34, C1QC, TLR9, ISG20, OASL2, NAIP5, OASL1, ZAP70, PSTPIP1, FCER1G, CLEC4A2, MR1, CSF1R, TYROBP, ZBP1, ITK, CARD9, HCK, PIK3CD, PADI4, TRIL, FCGR1, IFIT3, CD84, C1QA, IFIT2, C1QB, CYBB, C1RL, TXK, TREM2, RNF135

Gene Ontology enrichment analysis of differentially regulated transcripts from the Ric^{EKO} versus control comparison by using DAVID 6.8 online software. Only genes that have a fold change of greater than 1.5 and a *P* value of less than .05 were used.